Materials & Design 267 (2026) 116244

Contents lists available at ScienceDirect

Materials & Design

journal homepage: www.elsevier.com/locate/matdes

Visible light-mediated crosslinked methacrylated gellan gum nanocomposite hydrogel: physicochemical characterization and *in vivo* safety

Giorgia Codispoti [a,1], Diego Trucco [b,c,*,1], Melania Carniato [d], Lorenzo Vannozzi [b,c], Lucia Martini [a], Cristina Manferdini [e], Gina Lisignoli [e], Matilde Tschon [a,*], Milena Fini [f], Leonardo Ricotti [b,c]

[a] Surgical Sciences and Technologies, IRCCS Istituto Ortopedico Rizzoli, Via di Barbiano, 1/10, Bologna 40136, Italy
[b] The BioRobotics Institute, Scuola Superiore Sant'Anna, Piazza Martiri della Libertà, 33, Pisa 56127, Italy
[c] Department of Excellence in Robotics & AI, Scuola Superiore Sant'Anna, Piazza Martiri della Libertà, 33, Pisa 56127, Italy
[d] Department of Veterinary Medical Sciences, University of Bologna, Via Tolara di Sopra, 43, Bologna 40064, Italy
[e] Laboratory of Immunorheumatology and Tissue Regeneration, IRCCS Istituto Ortopedico Rizzoli, Via di Barbiano, 1/10, Bologna 40136, Italy
[f] Scientific Director, IRCCS Istituto Ortopedico Rizzoli, Via di Barbiano, 1/10, Bologna 40136, Italy

ARTICLE INFO

Keywords:
Methacrylatedgellan gum hydrogel
Functional nanomaterials
Preclinical biocompatibility
In vivo safety
Visible-light photocrosslinking

ABSTRACT

Methacrylated gellan gum (GGMA) injectable hydrogels have emerged as promising candidates for cartilage tissue engineering due to their structural similarity to cartilage glycosaminoglycans and the tunability enabled by visible-light photocrosslinking. Incorporating functional nanomaterials represents a promising approach to improve their functionality for cartilage repair. Although several studies have highlighted the *in vitro* potential of nanocomposite hydrogels, comprehensive evaluations of the *in vivo* safety of photocrosslinkable hydrogels for clinical use remain limited. Here, we demonstrated that the incorporation of graphene oxide nanoflakes and barium titanate nanoparticles into visible light–crosslinked GGMA hydrogels preserved their shear-thinning behavior while improving mechanical properties and adhesion to cartilage, without affecting lubrication or degradation. *In vitro* safety, evaluated according to ISO 10993 standards, confirmed the absence of cytotoxicity in human chondrocytes and genotoxic effects both in bacteria and human lymphoblasts. *In vivo* ISO 10993-compliant assessments (including skin irritation, delayed-type hypersensitivity, acute and subchronic systemic toxicity, and local effects after implantation) confirmed the biocompatibility of GGMA nanocomposites, with no local or systemic adverse effects in both animal sexes. Overall, GGMA-based nanocomposite hydrogels exhibited favorable mechanical and biological properties and a safe *in vivo* profile, supporting their potential for translational cartilage applications.

1. Introduction

Articular cartilage (AC) can be damaged by trauma, mechanical overload, overuse or aging, and, although early lesions may repair with fibrocartilage, this tissue has inferior quality and limited regenerative capacity [1,2]. If the defect is not repaired, extracellular matrix (ECM) degradation may extend to the subchondral bone, promoting inflammation, chondrocyte apoptosis, and, in the last instance, leading to osteoarthritis (OA) [3–5]. Patients experience chronic pain, swelling, joint dysfunction, and reduced mobility, resulting in chronic disability, social isolation, and a worsening of quality of life, resulting also in increased direct and indirect healthcare costs [6–8]. Although surgical options offer some benefit, their outcomes remain suboptimal [9]. For this reason, research is increasingly focusing on tissue engineering strategies, particularly on hydrogels [10,11]. These highly hydrated polymeric networks may mimic native cartilage, ensuring biocompatibility and reducing inflammation. They also allow drug loading and can be mechanically tuned to support joint function. Furthermore, they can

* Corresponding authorsat: Dr. Matilde Tschon: Surgical Sciences and Technologies, IRCCS Istituto Ortopedico Rizzoli, Via di Barbiano, 1/10, Bologna 40136, Italy.
E-mail addresses: diego.trucco@santannapisa.it (D. Trucco), matilde.tschon@ior.it (M. Tschon).
[1] Equally contributing.

https://doi.org/10.1016/j.matdes.2026.116244
Received 28 November 2025; Received in revised form 5 May 2026; Accepted 15 May 2026
Available online 16 May 2026

be delivered minimally invasively, enriched with orthobiologics to promote chondrogenesis, and engineered as smart hydrogels capable of adaptive, stimulus-responsive drug release [12]. Building on these hydrogel advantages, gellan gum (GG), an anionic polysaccharide produced by *Sphingomonas elodea*, has emerged as a highly promising platform in tissue engineering thanks to its biocompatibility and tunable mechanical properties [13–15]. Its backbone, rich in glucuronic acid, mimics the glycosaminoglycans naturally present in articular cartilage. In addition, its thermosensitive behaviour and ion-mediated gelation allow for shear-thinning injectability and rapid gelation under physiological conditions. These properties made it a highly promising material for cartilage tissue engineering [14–16]. GG can be chemically modified into methacrylated gellan gum (GGMA), enabling both physical and chemical crosslinking to finely-tune its network density [17–19]. Unlike temperature-sensitive GG, GGMA is water-soluble at room temperature, injectable, and can undergo photocrosslinking with UV or visible light, underlining its potential *in vivo* and in clinical applicability [15,20,21].

While crosslinking parameters, as photoinitiator concentration and light dose, can be tuned to modulate the degree of hydrogel crosslinking, thus their mechanical properties, additional functionalities can be introduced them through the integration of specific functional nanomaterials [22,23]. In this context, piezoelectric inorganic nanomaterials offer the potential to stimulate bioeffects in human cells [24]. Among these, barium titanate nanoparticles (BTNPs) represent a state-of-the-art piezoelectric material, exhibiting superior piezoelectric activity compared to natural counterparts [25,26]. Several studies have demonstrated the ability of such materials to promote the differentiation of adipose-derived stem cells into chondrocyte-like phenotype, to enhance early myogenesis in skeletal muscle cells, and other bioeffects [27,28]. In parallel, carbon-based nanomaterials have attracted attention due to their unique morphological and chemical properties, which can enhance the mechanical strength and lubrication characteristics of hydrogels while also modulating cellular behaviour [29]. Graphene oxide (GO), in particular, has been shown to improve hydrogel toughness, increase lubrication and resistance to wear, and serve as a platform for growth factor binding to shape a favourable chondrogenic microenvironment [30–32]. A tailored cocktail of piezoelectric (50 μg/mL) and carbon-based (25 μg/mL) nanomaterials, consisting of BTNPs and GO, was previously integrated into an ultrasound-stimulated, ionically crosslinked hydrogel (VitroGel-RGD®) to support the chondrogenic differentiation of adipose-derived stem cells toward a pro-chondrogenic phenotype [27,33].

Despite the increasing interest in the integration of functional nanomaterials into hydrogels, comprehensive evaluations of the *in vivo* safety profile of composite photocrosslinkable hydrogels remain limited. Visible light-mediated crosslinking represents a safer alternative to UV-based approaches, improving cytocompatibility and supporting translational safety, whereas UV irradiation may raise concerns about potential cytotoxic effects due to DNA damage [34]. In parallel, the concurrent incorporation of BTNPs and GO allows to take advantage of complementary contributions: BTNPs provide mechanical reinforcement and potential piezoelectric responsiveness, while GO contributes to mechanically strengthen the hydrogel, enhance interfacial interactions and adhesion with the cartilage, and contribute to friction reduction. This synergistic improvement of properties is rarely achieved in hydrogels in the absence of nanofillers [35], although this added degree complexity underlines the importance of understanding the nanofiller behavior and safety *in vivo*. As *in vitro* studies can only give a partial indication of the potential biocompatibility of nanomaterials embedded within hydrogels, a deeper understanding of genotoxicity and both short-term and long-term *in vivo* safety is essential to identify potential adverse effects associated with the implantation of nanocomposite hydrogels (e.g., bioaccumulation of nanomaterials, or triggering of immune response [36]) and ensure a safe use in future clinical applications. This gap in the current knowledge poses a significant barrier to clinical translation of nanocomposite hydrogels for applications requiring *in vivo* implantation.

This study aimed to investigate the functional characteristics of visible light-crosslinked GGMA-based hydrogels doped with BTNPs and GO nanoflakes, and their *in vivo* safety profile in accordance with ISO 10993 standards, as reported in the study design (Supplementary Table 1). We aimed to (i) develop and characterize a nanocomposite GGMA formulation tailored to articular cartilage lesion repair; (ii) evaluate its *in vitro* cytotoxicity and genotoxicity; (iii) investigate the *in vivo* safety and biocompatibility.

2. Materials and methods

2.1. Materials and reagents

Gellan gum (trademarked as Gelzan^{CM}), methacrylic anhydride (degree of purity: >94 %), phosphate-buffered saline without Ca^{2+}/Mg^{2+} (PBS), tris(2,2′-bipyridyl) ruthenium (II) chloride hexahydrate (Ru, 99.95 % trace metals basis), sodium persulfate (SPS, degree of purity: >98 %), Fetal Bovine Serum (FBS), lysozyme, sodium azide (NaN_3), ethylenediaminetetraacetic acid (EDTA), and hydrogen peroxide (H_2O_2) were purchased from Sigma-Aldrich Merck (USA). Dialyzing membranes (MWCO 12–14 kDa) were purchased from CelluSep (USA). Propyl glycol alginate (PGA, degree of esterification <80%) was purchased by Carbosynth (Staad, St. Gallen, Switzerland), while dopamine hydrochloride and sodium hydroxide (NaOH) were purchased by Sigma-Aldrich Merck (USA). Human chondrocytes (cod. 402–05a) and their culture growth medium (cod. 411–500) were purchased from Cell Applications, Inc. (USA). Live/Dead (L/D) kit was purchased from Life Technologies (USA). PrestoBlue and Lactate Dehydrogenase kits were purchased from Invitrogen (USA). The Ames MPF Penta II kit (cod. B10-513-S2-P) for the bacterial reverse mutation assay (Ames test) was obtained from Xenometrix AG (Switzerland). For the micronuclei test, the human lymphoblastoid TK6 cell line was purchased from the American Type Culture Collection (cod. CRL-8015, ATCC, USA), while the RPMI 1640 medium and the Dulbecco's phosphate-buffered saline (DPBS) were acquired from Euroclone S.p.A. (Italy). For *in vivo* tests, male and female White New Zealand rabbits, Dunkey-Hurtley guinea pigs and Sprague-Dawley rats were purchased from Charles River Laboratories (Italy). Physiological saline solution was sourced from Fresenius Kabi (Italy), sodium dodecyl sulfate (SDS, cod. 15525017) from Invitrogen (USA), Freund's complete adjuvant (FCA, cod. F-5881) and α-hexylcinnamaldehyde (cod. 291285) from Sigma-Aldrich, Merck. Ketamine Imalgene 1000 from Boehringer Ingelheim Animal Health Italia S.p.A. (Italy), Xylazine Rompun 25 ml from Bayer S.p.A. (Italy), and Tanax® from Hoechst AG (Germany). Nitric acid (HNO_3) was obtained from Carlo Erba (Italy), and the DigiPrep digestion system from SCP-Science QuantAnalitica SRL (Italy). Standard solutions of barium (Ba) and titanium (Ti) from CPA Chem (Italy). Xylene was obtained from VWR Chemicals (Italy), paraffin Lab-O-Wax Plus from Histoline (Italy), Mayer's Hematoxylin Solution from Sigma-Aldrich (Merck), Eosin Y-solution 0.5% aqueous from Carlo Erba (Italy). Hymovis® was provided by Fidia Farmaceutici (Italy), and Testsimplets® slides were obtained from Waldeck (Germany). Instruments used included the Aperio Scanscope Digital Scanner AT2 (Leica Biosystems, Germany), Microm HM355 S (ThermoFisher Scientific), and MassHunter 4.2 Software (Agilent Technologies, USA).

2.2. Nanomaterial and GGMA preparation

Barium titanate nanoparticles (BTNPs) were prepared via hydrothermal synthesis [27,28], while Graphene Oxide (GO) nanoflakes were prepared following a modified Hummers' method [37,38]. Both BTNPs and GO were autoclaved through vapor steam (30 min at 121°C and 1 bar), ensuring their sterilization according to ISO 17665-1 (2006). Afterwards, a polymer wrapping step was conducted on both BTNPs and GO using propylene glycol alginate (PGA) and polydopamine (PD), as

previously described [27,33]. Briefly, autoclaved GO (5 mg/mL) was dispersed in an aqueous dopamine hydrochloride solution at 5 mg/mL, prepared in deionized water (d-H2O) previously filtered (0.22 μm, PES) and adjusted to pH 8.5 by dropwise addition of 1 M NaOH. The suspension was subjected to probe sonication (25 W, 300 s, 20 kHz, Bandelin SonoPuls HD4050, Berlin, Germany) and subsequently stirred vigorously for 24 h at room temperature under dark conditions. A PGA solution was prepared at 2.5 mg/mL in d-H2O and filtered (0.22 μm, PES) at RT. Autoclaved BTNPs were then added to the polymer solution at a 1:1 w/w ratio and the mixture was processed by probe sonication (25 W, 30 min, 20 kHz; Bandelin SonoPuls HD4050, Berlin, Germany).

The methacrylation of GG was carried out similarly to Coutinho *et al.* [39], as described in our previous studies [21,40,41]. Briefly, 1% w/v gellan gum (GG) was dissolved in d-H_2O at 75°C under stirring for 1 h, then cooled to 60°C before the slow addition of methacrylic anhydride (MA) (8.5 mL per 100 mL of solution). The mixture was maintained at pH 8–9 for 6 h by constantly adding droplets of NaOH dissolved in d-H_2O at 1 M and reading the pH with a pH meter (Hanna Instruments, Italy). Then, the unreacted anhydride was removed by centrifugation (3500 rpm, 3 min at 30°C). The supernatant was diluted 1:2 with d-H_2O pre-heated to 40°C, dialyzed at 60°C for 5 days, rapidly frozen, and stored at −80°C. Lyophilization over 3 days yielded the methacrylated gellan gum (GGMA) powder, which was kept at −80°C until use. Sterilization was achieved by vapor steam autoclaving (30 min at 121°C, 1 bar) in accordance with ISO 17665-1 (2006). For the photo-crosslinking, stock solutions of ruthenium (Ru, 20 mM) and sodium persulfate (SPS, 200 mM) were prepared in water and stored at 4°C until use.

2.3. Nanomaterials characterization

Piezoelectric Force Microscopy (PFM) was employed to assess the piezoelectric properties of BTNPs and evaluate the piezoelectric responsiveness of nanocomposite hydrogels. Briefly, 10 μL of BTNP suspensions (50 μg/mL) were drop-cast onto an indium tin oxide (ITO)-coated polyethylene terephthalate (PET) substrate substrate and allowed to dry at room temperature under a chemical hood. In contrast, *GGMA nanocomp* hydrogels were allowed to dehydrate onto the ITO-PET substrate before measurements. Measurements were conducted using an AFM operating in Peak Force PFM mode (Dimension Icon, Bruker, USA), over a scan area of 1 μm^2 with a scan frequency of 0.3 Hz. An antimony (n)-doped silicon cantilever with platinum–iridium coating (SCM-PIT-V2, Bruker), characterized by a spring constant of 2.5 N/m, a resonant frequency of 70 kHz, and a deflection sensitivity of 112 nm/V, was used.

The analysis was performed by applying an AC voltage (V_{ac}) of 2 V at 59 kHz, i.e., outside the cantilever resonance frequency, to probe the out-of-plane (vertical) piezoresponse. The piezoelectric activity was analysed from the PFM maps by quantifying the displacement amplitude (pm) induced in the material upon electrical excitation. For BTNPs, the effective d_{33} coefficient was calculated as:

$$d_{33} = \gamma \frac{A}{V_{ac}} \tag{1}$$

where γ represents a correction factor, A is the measured amplitude (pm), and V_{ac} is the applied AC voltage (V). Calibration of γ was performed using a polyvinylidene fluoride (PVDF) thin film reference sample (Goodfellow; thickness: 28 μm; $d_{33} \approx -20$ pC/N). To evaluate the ferroelectric behavior of the BTNPs, a DC bias sweep (±10 V, scan frequency 0.1 Hz) was applied to the tip. In this case, the excitation frequency was set to 70 kHz, close to the cantilever resonance, to enhance measurement sensitivity.

2.4. Preparation of bare GGMA and GGMA nanocomp hydrogels

GGMA hydrogels were prepared following the optimized formulation selected in our previous work [21]. Briefly, lyophilized GGMA powder was dissolved in PBS at 37 °C in a water bath at a concentration of 2% w/v. Then, Ru (0.1 mM) and SPS (1 mM) were added to the GGMA solutions to enable the matrix photo-crosslinking in response to light. GO nanoflakes and BTNPs were added at concentrations of 25 and 50 μg/mL, respectively, and gently mixed. Then, 200 μL of the pre-crosslinked GGMA solution was gently transferred into a cell crown (Scaffdex, Merck, USA) inserted into a 24-well plate. Each cell crown was previously prepared by blocking a polystyrene membrane (diameter: 10 mm, Goodfellow, UK) obtained by punching it with a biopsy tool (diameter: 10 mm, SMI AG, Belgium). All hydrogels were cross-linked using a white LED source (RfQ – Medizintechnik, GmbH & Co), featured by a spectrum with a peak at 450 nm. The light was applied with an intensity of 18 $mW \cdot cm^{-2}$ for 60 s, as previously optimized by our group [21]. From this point, the bare GGMA hydrogels were named *GGMA*, while the nanocomposite GGMA hydrogels were named *GGMA nanocomp*.

2.5. Rheological characterization

The rheological characterization was carried out on the pre-crosslinked solution of *GGMA nanocomp* and *GGMA* using a rheometer (Anton Paar MCR-302, Graz, Austria) with a cone-plate geometry (diameter: 25 mm, angle = 1°). The flow curves were acquired at room temperature (25 °C) at shear rates ranging from 0.1 to 1000 s^{-1} in rate-controlled mode by selecting 10 points for each decade. The dynamic viscosity (*η)* was modelled as a non-Newtonian fluid according to the following power law (2) [42]:

$$\eta = K\dot{\gamma}n^{-1} \tag{2}$$

where $\dot{\gamma}$ is the fluid shear rate, *K* the consistency index, and *n* the flow behaviour index. *K* and *n* were determined from each shear rate sweep rheometric curves through linear interpolation.

The shear stress (τ) applied to cells during injection within the hydrogel solution can be analytically estimated using the previously calculated rheological indexes, n and K, derived from each rheological flow curve. This estimation considers the injection parameters, such as the inner diameter (d) of clinically compatible needles, which range from 18G to 24G, and the flow rate (Q = 5.8 mm/s), as outlined in ISO 7886-1 (2018). The estimation follows Equation (3) as reported in previous works [27,43]:

$$\tau = -K\frac{d}{2}\left[Q\left(\frac{3n+1}{n}\right)\left(\frac{d}{2}\right)^{\frac{3n+1}{n}}\right]^n \tag{3}$$

2.6. Morphological, sol fraction, and swelling analysis

The network architecture of *GGMA* and *GGMA nanocomp* hydrogels was compared by Scanning Electron Microscopy (SEM). The upper top and cross-sections of photo-crosslinked hydrogels were coated with an 8 nm platinum (Pt) layer via RF/DC magnetron sputtering (Kenosistec) under vacuum (70 W, 0.02 bar, 10 s, static mode). Imaging was performed using a SEM (Phenom XL, Thermo Fisher, USA) under high vacuum, with an accelerating voltage of 15 kV, employing a Secondary Electron Detector (SED) in point mode.

The sol fraction was evaluated to assess the crosslinking efficiency of both *GGMA* and *GGMA nanocomp* hydrogels. Following hydrogel preparation, the sol fraction (%) was calculated as:

$$\text{Sol fraction}\,(\%) = \frac{W_{dry1} - W_{dry2}}{W_{dry1}} \times 100 \tag{4}$$

where W_{dry1} and W_{dry2} correspond to the sample weights after the first and second lyophilization steps, respectively.

Additionally, photo-crosslinked *GGMA* and *GGMA nanocomp* hydrogels were incubated in PBS at 37 °C and 5% CO_2 for up to 48 h to assess their swelling over time. Samples were weighed immediately after photo-crosslinking, at 24 h, and 48 h. The swelling was calculated as:

$$S_t(\%) = \frac{w_t - w_0}{w_0} \times 100 \quad (5)$$

where w_t represents the rinsed hydrogel weight at each time point, and w_0 is the initial weight measured immediately after photo-crosslinking.

2.7. Adhesion to the cartilage test, mechanical and tribological characterization

The adhesion strength of photo-crosslinked *GGMA* and *GGMA nanocomp* to the cartilage tissue was assessed using a setup reported in [27,40] and shown in Supplementary Fig. S1a. Briefly, the setup was designed by printing (Visijet M3 Crystal, ProJet MJP 3600) a spline-mounted fixture for a traction test machine (Instron 2444) to quantify hydrogel–cartilage adhesion. The bottom base anchors to the machine, while two cartilage holders (Ø: 6.4 mm × h: 7 mm) clamp bovine knee biopsies (Ø: 6.4 mm × h: 10 mm). A top hydrogel holder (Ø: 15 mm × h: 5 mm) attaches to the ± 10 N load cell and permits direct pouring of 400 μL hydrogel solution atop the cartilage. After *in situ* photo-crosslinking, tensile tests are run at 1 mm min^{-1} until failure. Peak adhesion strength (expressed in kPa) was calculated as maximum force divided by contact area.

Uniaxial compression tests were performed on photo-crosslinked *GGMA* and *GGMA nanocomp* samples using a traction test machine (Instron 2444), applying a compression rate of 1 mm s^{-1}. Until the mechanical characterization, the samples were kept in PBS at 37°C for 24 h. The compressive elastic modulus (*E*) was calculated from the linear region of the strain-stress curve (initial 10% of the linear region), fitted according to the equations:

$$\sigma = \frac{F}{A_0} \quad (6)$$

and

$$\varepsilon = \frac{\Delta l}{l_0} \quad (7)$$

where σ is the stress and ε is the strain, F is the force, Δl is the deformation, A_0 is the sample initial cross-sectional area, and l_0 is the sample initial length. E was calculated according to the equation:

$$E = \frac{\sigma}{\varepsilon} \quad (8)$$

Tribological characterization of the crosslinked hydrogels was carried out on an MCR 102 rheometer (Anton Paar, Austria) fitted with a Tribocell T-PTD200 (including the H-PTD200 hood, Peltier temperature control, and disposable shaft), according to [30]. Custom holders locked each hydrogel specimen beneath a flat, borosilicate glass disc mounted to the rotating shaft. Under a constant normal load of 0.5 N (≈6.4 kPa contact pressure), the coefficient of friction (COF), as the ratio of tangential (frictional) to normal force, was measured at 37°C in the transition point between static and dynamic regimes. Two lubricants were tested: PBS and an ISO 14243–compliant synthetic synovial fluid (25% sterile FBS in water, 0.2% NaN_3, 20 mM EDTA). For each lubricant, three full Stribeck curves were generated for each sample by logarithmically ramping rotational speed from 10^{-5} to 10^{2} min^{-1} under a constant 0.5 N load. Wear resistance was assessed in a separate run by holding the speed at 5 min^{-1} for 30 minutes.

2.8. Degradation analysis

Degradation analysis was performed to evaluate hydrogel stability under physiological and osteoarthritic-like conditions. *GGMA* and *GGMA nanocomp* hydrogels were incubated at 37°C in PBS, PBS with lysozyme (120 μg/mL), or ISO 14243–compliant synthetic synovial fluid. At 15, 30, and 60 days, samples were removed, rinsed, blotted dry, and weighed. The percentage mass loss was calculated as:

$$Mass(\%) = \frac{W_0 - W_t}{W_0} \times 100 \quad (9)$$

where W_0 is the initial dry mass and W_t is the dry mass at time *t*.

2.9. In vitro biological characterization

2.9.1. Cell viability, metabolic activity and cytotoxicity

Human chondrocytes (HCs) were thawed and expanded in their cell culture growth medium up to passage 4. HCs were gently added to the *GGMA nanocomp* solution at a density of 2 × 10^6 cells/mL in a 50 mL tube and mixed with a viscous solution pipette (Microman m1000E, Gilson, USA). Then, the cell-laden solution was cast in cell crowns (Scaffdex, Merck, USA) mounting a polystyrene membrane (diameter: 10 mm, Goodfellow, UK) and photo-crosslinked under a white LED source (RfQ – Medizintechnik, GmbH & Co.) for 60 s at 18 mW·cm^{-2}. The hydrogels with the final dimension given by the cell crown (diameter: 10 mm, height: 2 mm) were cultured at 37 °C with 5% CO_2, and the cell culture growth medium was changed daily. Viability, metabolic activity, and cytotoxicity of HCs embedded within *GGMA nanocomp* were assessed at 2, 7, and 14 days on independent samples. Viability was determined using the Live/Dead® kit, following the manufacturer's instructions, and visualized by confocal fluorescence microscopy (Leica, Stellaris, Germany). The percentage of live cells was estimated using ImageJ.

Metabolic activity was measured using PrestoBlue® (10% v/v, 3 h incubation), with fluorescence recorded at 590 nm (Victor Nivo, PerkinElmer, USA). Cytotoxicity was quantified from culture supernatants using an LDH assay kit, according to the manufacturer's instructions, with absorbance measured at 490 nm and results expressed as percent cytotoxicity.

2.9.2. Genotoxicity tests

The purpose of genotoxicity testing is to identify substances capable of inducing (point) genetic mutations or structural or numerical chromosome damage. In *vitro* genotoxicity tests were performed as a battery of tests in accordance with ISO 10993-3 (2015), by the Ames test on bacterial cell systems and the micronucleus test on mammalian cells.

2.9.2.1. Ames test. The Ames bacterial reverse mutation assay was performed using six serial concentrations (C) of *GGMA nanocomp* (C1: 0.03125X; C2: 0.0625X; C3: 0.125X; C4: 0.25X; C5: 0.5X and C6: 1X), as well as the cross-linked solid form. Four strains of *Salmonella typhimurium* (TA98, TA100, TA1535, and TA1537) and one strain of *Escherichia coli* (WP2 *uvrA* [*pKM101*]) were exposed to the nanocomposite either in disaggregated form (C1-C6) or as a solid hydrogel, both in the presence and absence of the metabolic activator (Aroclor 1254-induced rat liver S9 fraction). After a 24-hour incubation, the bacterial strains were exposed to varying concentrations of *GGMA nanocomp*, alongside positive and negative controls. Following exposure, the bacterial cultures were incubated in histidine- or tryptophan-lacking medium, according to their specific growth conditions, and transferred to 384-well plates. The plates were then incubated at 37 °C for 48 hours. After incubation, the number of reverted colonies was counted: wells with unreverted colonies appeared purple-blue, while reverted colonies displayed a yellow colour. The number of positive wells for each concentration, tested in triplicate, was compared to the spontaneous revertants observed in the negative control. Positive controls were used to validate the assay with and without the S9 fraction.

2.9.2.2. Micronuclei test. The micronuclei assay was conducted using the human lymphoblastoid TK6 cell line. Cells were seeded (0.25 × 10^6 cells/well) into 6-well plates and exposed to three different concentrations of *GGMA nanocomp* (1.25X, 1X, and 0.75X) for periods of 3 and 24 hours, as well as negative (fresh medium) and positive (0.5 mg/mL

H_2O_2) controls, with each experimental condition performed in duplicate. Following exposure, cells were collected and resuspended at a concentration of 1×10^5 cells/mL in RPMI1640 medium for a subsequent 40-hour recovery period; thereafter, cell counts were performed to assess population doublings. Duplicate slides for each nanocomposite concentration and control group were prepared, stained with a 4% Giemsa solution in water, and digitalized using the Aperio Scanscope Digital Scanner AT2. Micronuclei (MN) frequencies were analysed at high magnification (400–1000X) and scored in 1000 cells per slide. Population Doubling (10) and Relative population doubling (RPD) (11) were calculated to estimate the cytotoxic activity of the treatment as follows:

$$Population\ Doubling = \frac{\log\left(\frac{n.\ of\ cells\ post\text{-}treatment}{n.\ of\ cells\ before\ treatment}\right)}{\log(2)} \quad (10)$$

$$RPD = \frac{n.\ of\ population\ doubling\ in\ treated\ cultures}{n.\ of\ population\ doubling\ in\ control\ cultures} \times 100 \quad (11)$$

2.10. In vivo safety and biocompatibility evaluations

To assess the biocompatibility of *GGMA nanocomp*, the following *in vivo* tests were performed in accordance with ISO 10993: (i) skin irritation test; (ii) delayed-type hypersensitivity test; (iii) acute and subchronic systemic toxicity tests; (iv) local effects after implantation test.

The project was firstly approved by the Animal Welfare Body of the Rizzoli Orthopaedic Institute (Bologna, Italy) and then authorised by the Italian Ministry of Health (No. 777/2021-PR) on October 28th, 2021. All *in vivo* experiments were carried out in full compliance with Italian regulations on the protection of animals used for scientific purposes (Legislative Decree No. 26/2014), as well as with the European Commission's Recommendation 2007/526/EC on guidelines for the housing and care of animals used in experimental and other scientific contexts. The sample size for each test was specified in ISO 10993 standards. Experimental protocols were designed in accordance with the Planning Research and Experimental Procedures on Animals: Recommendations for Excellence (PREPARE) guideline [44], and the study was reported following the standards set by the *Animal Research: Reporting of In Vivo Experiments* (ARRIVE) guideline [45]. Animal acclimatization was performed using a 10-day quarantine. Humane endpoints for avoiding animal distress included body weight loss exceeding 20% relative to the physiological growth curve, severe limb injuries or irreversible impairments in general health or vital organ function, and the occurrence of intense, pharmacologically unmanageable pain. After test completion, animals used for the skin irritation, sensitisation, and acute systemic toxicity tests were reintegrated into the facilities for the rehabilitation and reintegration of animals used for scientific purposes (La Collina dei Conigli Onlus, Italy).

Before these evaluations, the exposure time required for *in vivo* photo-crosslinking of *GGMA nanocomp* was determined by measuring light attenuation through an *ex vivo* skin layer placed between the light source and a calibrated dosimeter, and comparing the transmitted light with *in vitro* conditions. The *in vitro* photocrosslinking protocol was performed at an intensity of 18 mW·cm^{-2} for 60 s. An attenuation factor of 3.97 was measured through skin; therefore, to deliver a comparable dose at the target site *in vivo*, the irradiation time was increased approximately fourfold while maintaining the same intensity at the source (18 mW·cm^{-2} for 240 s). Increasing exposure time rather than intensity was selected to minimize potential local heating and reduce the risk of thermal effects in living tissues (subcutaneous layers and joint space). Accordingly, injection sites were irradiated with visible light for 240 s at a distance of 1.5 cm from the animal skin surface.

2.10.1. Skin irritation test

Skin irritation test was performed on four male New Zealand Specific-pathogen-free (SPF) rabbits (basal weight 2.6 ± 0.2 kg) according to ISO 10993-23 (2021). Four patches soaked in *GGMA nanocomp,* negative control (physiological saline solution) and SDS, a known positive sensitiser, were topically applied to the hair-trimmed back region of rabbits. After 4 hours of exposure, the treated areas were scored for erythema and oedema at 1, 24, 48, and 72 hours. The primary irritation index (PII) (minimum 0 to maximum 8) was calculated and recorded according to the ISO 10993-23 (2021) standard.

2.10.2. Delayed-type hypersensitivity test

The Guinea Pig Maximization Test (GPMT) was chosen for its high sensitivity in detecting sensitizing substances, as reported in ISO 10993-10 (2010). Twenty-three Dunkin Hartley guinea pigs of both sexes, with a mean body weight of 387.6 ± 20.8 g for males and 367.4 ± 14.0 g for females, were utilized. In preliminary tests, three animals were used to determine the undiluted optimal dose of the *GGMA nanocomp*. The main test was carried out in two phases: induction and challenge. First, animals received intradermal injections in a shaved area on their backs, using different formulations of *GGMA nanocomp*, negative (saline solution), and positive controls (5% α-hexylcinnamaldehyde). One week later, patches with the test substance, a positive or negative control, were applied for a further 48 hours. Two weeks later, in the challenge phase, the same substances were reapplied to a different area (left flank) for 24 hours. Skin reactions were evaluated at 24 and 48 hours using a standard scoring system to assess erythema and swelling, according to the Magnusson and Kligman grading scale [46].

2.10.3. Acute and subchronic systemic toxicity

Acute and subchronic systemic toxicity tests were performed according to ISO 10993-11 (2018) in Sprague-Dawley rats. The acute systemic toxicity test was performed on ten male rats (basal weight 340.4 ± 17.6 g): five rats were injected intramuscularly with *GGMA nanocomp* in the left thigh and the others with saline solution as a negative control group. After injection, the *GGMA nanocomp*-treated thighs were irradiated for the nanocomposite hydrogel photocrosslinking. The onset of clinical signs of major body systems (neurological, respiratory, cardiovascular, gastrointestinal, urinary, musculoskeletal, ocular), body weight measurements, and water and food intake were assessed and recorded at baseline and at 24, 48, and 72 hours. A symptom scoring sheet was completed and recorded for each animal at all time points.

The subchronic systemic toxicity test was performed on forty male and female rats (weight males and females 293.6 ± 23.5 g and 253.2 ± 16.3 g, respectively): twenty animals, ten males and ten females, were intraarticularly treated with *GGMA nanocomp*, while the other twenty were used as a negative control group (CTR–, saline solution). Rats were weighed weekly and the onset of clinical signs in the main body systems as specified above. At the end of the 11 weeks, all animals were subjected to general deep anaesthesia induced by intramuscular injections of ketamine (44 mg/kg) and xylazine (0.3 mg/kg) and blood and urine samples were collected for haematological, biochemical, serum protein electrophoresis and urine analyses, respectively. Immediately, pharmacological euthanasia was performed by an intracardiac administration of 1 mL of Tanax® and the necroscopic evaluation was assessed. Main organs (brain, heart, thymus, lungs, liver, spleen, kidneys, uterus/ovaries, testis/epididymis) were explanted, weighed and processed for histology. Blood samples and organs for ICP-MS analysis were stored dry at −20 °C.

2.10.3.1. Inductively Coupled-Plasma Mass Spectrometry. To investigate the possible biodistribution of Ba and Ti chemical elements, ICP-MS analyses were performed on rat blood and organ samples from both female and male animals of CTR– and *GGMA nanocomp*-treated groups. Analyses were performed by Agilent 7700 ICP-MS equipped with an ASX-500 Series autosampler. Briefly, each sample was weighed at

approximately 3 ± 0.5 g in polypropylene tubes. Subsequently, 10 mL of HNO_3 (67–69 *v/v* % superpure) was added and samples were mineralized at 75 °C overnight in DigiPrep SCP-Science. The samples were then diluted with ultrapure water and filtered. Finally, before analysis by ICP-MS, the samples were further diluted with an acid solution of HNO_3 (2%) and HCl (0.5%). A reagent blank (HNO3 67–69%) and reference sample (Matrix reference material DLA58/2016) were tested for each set of samples analysed to ensure the reliability of results. Concentrations were calculated using a solvent calibration curve with a mixture of Ba and Ti standard solutions, ranging from 0.01 to 100 ng/mL. Internal laboratory standards were also continuously injected into the instrument during analysis to quantify the samples. The lower limit of quantification for Ti and Ba was set at 0.002 mg/kg.

2.10.4. Local effects after implantation test

The local effects after implantation test were analysed according to ISO 10993-6 (2017). Ten male and ten female White New Zealand SPF rabbits (basal weight males and females 2.22 ± 0.15 kg and 2.37 ± 0.10 kg, respectively) were intra-articularly injected with *GGMA nanocomp* into the right knee, while the left knee was intra-articularly treated with Hymovis® hydrogel, as a clinically accepted medical device [47,48]. Knee joints treated with *GGMA nanocomp* were light irradiated for *GGMA nanocomp* crosslinking. At baseline and until the end of the experimental period of 3 months, animals were evaluated weekly for changes in weight and the onset of clinical signs. At the end of the experimental period, all animals were euthanized by an intravenous administration of 1 mL of Tanax® under deep general anaesthesia, as previously described, and synovial membranes, popliteal draining lymph nodes were processed for histology and synovial fluids were harvested. The synovial fluid was used for the quantification of the white blood cells (WBCs) by depositing 20 μL on slides pre-stained with Giemsa and then digitalized using Aperio Scanscope Digital Scanner AT2 at maximum magnification. A semiquantitative scoring system from Annex E of ISO 10993-6 (2016) was applied to synovial membrane slices for cellular and tissue response evaluation to *GGMA nanocomp* compared to Hymovis® in terms of the presence of cellular inflammatory infiltrate, fibrosis, necrosis, neovascularisation, and fatty infiltration.

2.10.5. Histological analyses

All samples for histology were first fixed in 10% buffered formalin solution for a minimum of 24 hours, dehydrated and embedded in paraffin. Sections with a thickness of 5 ± 1 μm were cut and stained with haematoxylin and eosin. All stained slides were digitally scanned at maximum magnification (40x) using an Aperio Scanscope Digital Scanner AT2.

2.11. Statistical analysis

All statistical evaluations for the *in vitro* and *in vivo* experiments were performed using GraphPad Prism (v 10.4.2). After having verified the normality with the Shapiro-Wilk test, normally distributed data were analysed using parametric tests and represented as mean ± standard deviation (SD), while data showing a non-normal distribution were analysed using non-parametric tests and represented as box plots, displaying the median, minimum, and maximum values. Experimental data on rheology (n = 4), COF (n = 4), degradation rate (n = 4), and *in vitro* metabolic activity (n = 3) and cytotoxicity (n = 4) were analysed by applying a nonparametric Kruskal−Wallis's test and Dunn's multiple comparison test. Data on sol fraction (n = 4), swelling over time (n = 4), compressive modulus (n = 4), and adhesion strength (n = 5) were analysed by applying a nonparametric Mann−Whitney U-test. The one-way ANOVA followed by a Sidak post hoc test was performed for the micronuclei dataset, while a two-way repeated-measures ANOVA (factors: treatment × time) followed by a Sidak post hoc test was used for the statistical analysis of longitudinal *in vivo* parameters, including animal body weight, food, and water consumption in the acute and subchronic systemic toxicity studies. Rheological flow curves, metabolic activities, and micronuclei datasets were represented as mean ± SD. Data on COF, degradation rate, cytotoxicity, adhesion strength, and compressive modulus were expressed as box plots, displaying the median, minimum, and maximum values. Significance was set at $p < 0.05$. For the other *in vivo* datasets, a Student's t-test was used to compare *GGMA nanocomp* levels with those of the negative control, with significance set at $p < 0.05$. Animals' parameters from acute and subchronic systemic toxicity evaluations were expressed as mean ± SD.

3. Results

3.1. Rheological characterization and injectability

Viscosity measurements were performed to assess whether the *GGMA* and *GGMA nanocomp* were suitable for safe cell injection with needle sizes compatible with clinical requirements. Fig. 1a–b presents the viscosity profiles of *GGMA* and *GGMA nanocomp* before (a) and after (b) crosslinking. The introduction of nanomaterials within *GGMA* resulted in a slight increase in viscosity without altering the shear-thinning behaviour. Only the consistency index (K) showed a significant increase after nanomaterial incorporation, both before and after crosslinking (Fig. 1c), while the flow index (n) remained unaffected (Fig. 1d). Fig. 1e reports the shear stress during injection of pre- and post-crosslinked hydrogels through 18–24 G needles, with values remaining below 50 Pa in all cases.

3.2. Piezoelectric response of BTNPs and GGMA nanocomp

PFM analysis confirmed the piezoelectric behavior of BTNPs, as shown in Supplementary Fig. S2a. The amplitude and phase responses as a function of the applied DC tip bias exhibited clear hysteresis loops (Supplementary Fig. S2b and c), consistent with ferroelectric/piezoelectric domain switching. Such non-linear electromechanical behavior is characteristic of piezoelectric ceramic materials. Quantitative analysis of the PFM data yielded an average d_{33} coefficient of 95.2 ± 13.6 pm/V, consistent with previously reported values for BTNPs [25,27].

Photo-crosslinked *GGMA nanocomp* hydrogels were also investigated by PFM. As shown in Supplementary Fig. S3, topography, amplitude, and phase maps acquired in the absence and presence of an applied bias (2 V) indicate a measurable electromechanical response under applied voltage. This behavior supports the presence of piezoelectric activity within the nanocomposite hydrogel thanks to the inclusion of BTNPs in the GGMA-based polymer network.

3.3. Morphological characterization and crosslinking-mechanical properties evaluation

SEM imaging revealed a homogeneous microstructure in both *GGMA* and *GGMA nanocomp* hydrogels, as shown in Fig. 2a from top and cross-sectional views. The lyophilization process sealed the network pores on the external surface of both hydrogels (Fig. 2a i-ii), while internally, they displayed an open porous architecture (Fig. 2a iii-iv). The addition of nanomaterials did not significantly change the pore size or morphology.

Sol fraction analysis indicated a statistically significant decrease upon nanomaterial incorporation. Specifically, *GGMA* showed a sol fraction of 10.76 ± 1.31%, while *GGMA nanocomp* reached 5.37 ± 2.22% (Fig. 2b). In aqueous environment (PBS), *GGMA* hydrogels exhibited higher swelling over time compared to *GGMA nanocomp*, as shown in Fig. 2c. Specifically, *GGMA* displayed a swelling of 35.30 ± 0.57% (24 h) and 37.41 ± 4.10% (48 h), whereas *GGMA nanocomp* showed lower values of 16.50 ± 3.35% and 20.20 ± 7.07% at the corresponding time points. These results indicate a consistently reduced swelling in the presence of nanomaterials, with statistically significant differences observed at both evaluated time points.

Following the photo-crosslinking degree of the sol fraction, the bulk

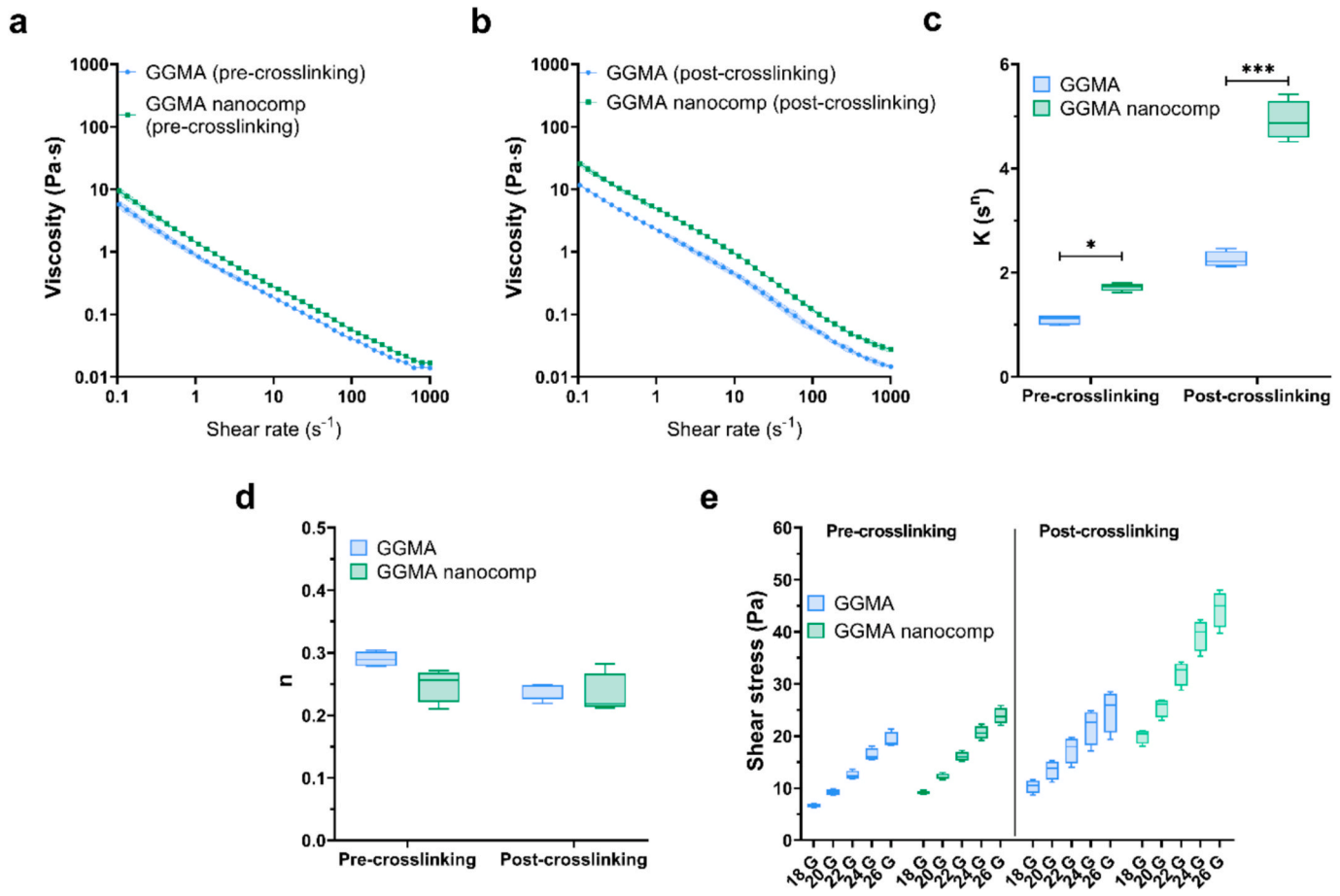

Fig. 1. Rheological characterization of GGMA and GGMA nanocomp. Flow curves of GGMA and GGMA nanocomp a) before and b) after the photo-crosslinking with a white LED source; mean ± SD, n = 4. Rheological indexes c) K and d) n extracted from each rheological flow curve of both pre- (left) and post- (right) crosslinked hydrogels throughout power law interpolation; data were expressed as box plots, displaying the median, minimum, and maximum values; Mann−Whitney U-test, n = 4, *p < 0.05; ***p < 0.001. e) Shear stress τ applied to cells during the injection of the pre-crosslinked (left) and post-crosslinked (right) hydrogel solutions within different gauges (G from 18 to 26) analytically calculated using Equation (3) interpolation; data were expressed as box plots, displaying the median, minimum, and maximum values; Kruskal−Wallis' test and Dunn's multiple comparison test, n = 4.

mechanical characterization via compression test showed a clear effect of nanomaterial incorporation: the compressive modulus increased from 0.89 ± 0.06 kPa for *GGMA* to 1.30 ± 0.17 kPa for *GGMA nanocomp*, with a statistically significant difference (*$p < 0.05$, Fig. 2d).

3.4. Adhesion to cartilage, tribological characterization, and degradation analysis

The adhesion strength was evaluated by photo-crosslinking the hydrogel solutions onto an *ex vivo* bovine cartilage sample (Supplementary Fig. S1b). As shown in Fig. 3a, the maximum adhesion strength of *GGMA* was 7.87 ± 1.25 kPa, while *GGMA nanocomp* resulted in a statistically significant improvement up to 13.28 ± 3.81 kPa. Additionally, *GGMA nanocomp* was retained onto the cartilage upon deposition (Supplementary Fig. 4a and b). The mechanical characterization of GGMA-based hydrogels was evaluated by measuring the compressive modulus (Fig. 3b).

The lubrication properties of *GGMA* and *GGMA nanocomp* were analysed in terms of COF, testing different lubricant solutions (PBS *vs* synthetic synovial fluid). Fig. 3b shows that the COF of *GGMA* was 0.022 ± 0.050 and 0.023 ± 0.006 in PBS and synthetic synovial fluid, respectively, while the COF of the *GGMA nanocomp* was 0.022 ± 0.0015 and 0.015 ± 0.003, respectively. In all cases, no statistical differences were found between hydrogels with and without nanomaterials across the different lubrication media (PBS and synthetic synovial fluid). The wear test showed that the COF did not vary over time in all cases and remained within 0.03 for up to 30 minutes (Fig. 3c).

Degradation analysis showed that both *GGMA* (Fig. 2d) and *GGMA nanocomp* (Fig. 2e) exhibited swelling behaviour, evidenced by a progressive mass increase from day 0 to day 15 under all tested conditions, except for the *GGMA nanocomp* incubated in synthetic synovial fluid, which displayed a slight mass decrease without statistical significance. On day 30, *GGMA* exhibited a statistically significant mass reduction in lysozyme and synthetic synovial fluid, whereas *GGMA nanocomp* showed a significant mass increase in the same environments. After 60 days, no statistically significant differences in mass were observed relative to the initial values for any of the tested conditions (Fig. 2d-e). These results likely reflect the enhanced mechanical properties of nanocomposite hydrogels compared to pure *GGMA*, attributable to increased crosslinking density induced by nanofillers, despite the inflammatory-mimicking environment.

3.5. In vitro biological characterization

3.5.1. Cell viability, metabolic activity, and cytotoxicity of HCs embedded into GGMA nanocomp

The *GGMA nanocomp* was evaluated biologically to assess its ability to support the viability of encapsulated cells. Cell viability was evaluated using the Live/Dead assay. As noticeable Fig. 4a, most labelled cells were alive (green) at all over such levels and at all time points (2, 7, and

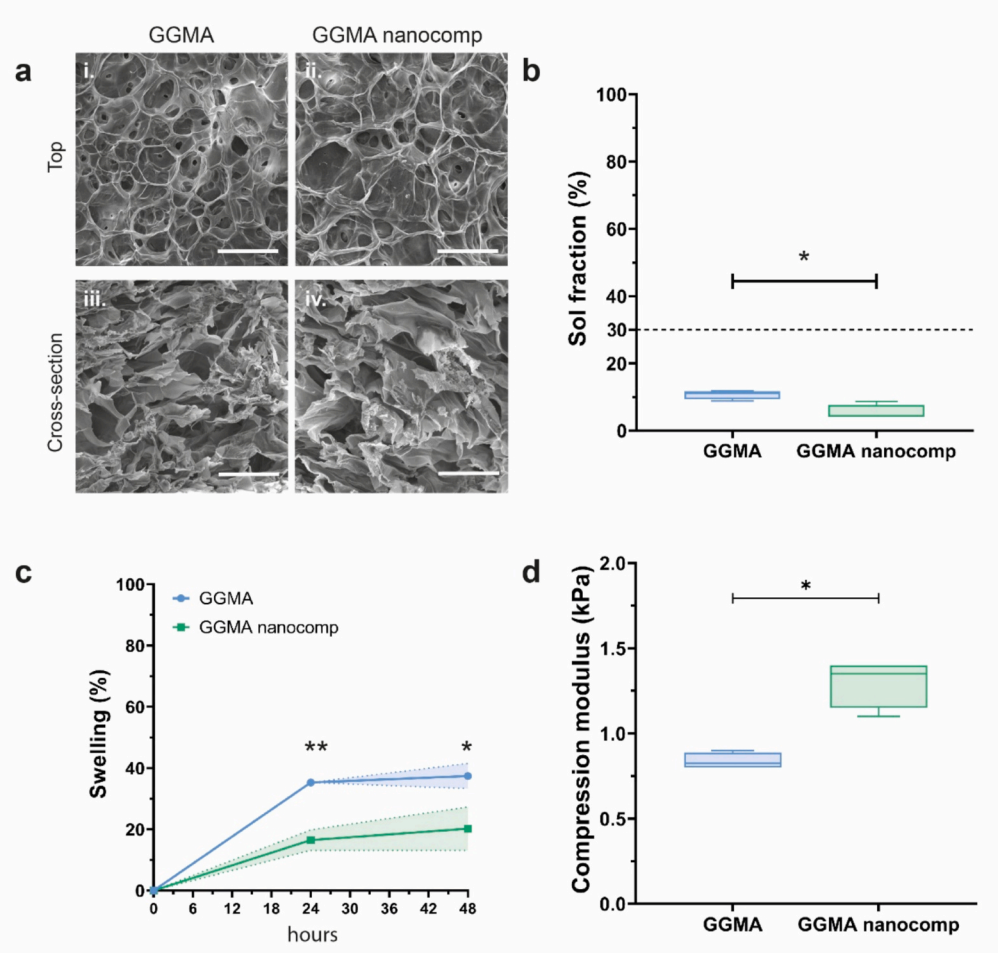

Fig. 2. Morphological and network characterization of photo-crosslinked GGMA and GGMA nanocomp hydrogels. a) SEM images of GGMA (i, iii) and GGMA nanocomp (ii, iv), shown from the top view (i, ii) and cross-sectional view (iii, iv) (scale bars: 300 μm). Comparative analysis between GGMA and GGMA nanocomp in terms of b) sol fraction, c) swelling in PBS over time (24 h and 48 h post-crosslinking), and d) compressive modulus. Data are presented as box plots showing median, minimum, and maximum values (n = 4). Data in c) are expressed as mean (dot points) and standard deviation (dashed lines). Statistical analysis was performed using the Mann–Whitney U test (*$p < 0.05$, **$p < 0.01$).

14 days after seeding). At day 14, a few dead red cells were present in the middle of the structure. The percentage of live cells was 98.3 ± 2.4%, 92.4 ± 8.7%, and 90.6 ± 4.7% at day 2, 7, and 14, respectively. Fig. 4b shows that the metabolic activity of *GGMA nanocomp* remained stable up to day 7, followed by an increase between days 7 and 14. The cytotoxicity was evaluated with the LDH kit, revealing an improvement in the LDH activity without a statistical difference from 13.68 ± 1.29% (day 2) to 20.78 ± 3.44% (day 7) (Fig. 4c).

3.5.2. Genotoxicity tests

3.5.2.1. Ames test. The Ames test showed that none of the tested concentrations of *GGMA nanocomp*, in its disaggregated (C1-C6) and solid cross-linked forms, exhibited mutagenicity. There was no concentration-response trend and/or a fold increase over baseline greater than 2.0 in any strain with or without metabolic activation (Supplementary Table 2 and Supplementary Table 3).

3.5.2.2. Micronuclei test. The micronuclei test on the TK6 cell line revealed that, following short (3 hours, Fig. 4d) or long-term exposure (24 hours, Fig. 4e) to the test substances, none of the three *GGMA nanocomp* concentrations (0.75x, 1x, and 1.25x) tested significantly increased MN frequencies compared to the negative control. However, positive controls always induced significant increases at both time points. So far, *GGMA nanocomp* has not caused chromosomal damage to TK6 cells.

3.6. In vivo safety and biocompatibility evaluations

3.6.1. Skin Irritation test

The Primary Irritation Index (PII) values obtained from the skin irritation test, based on the oedema and erythema scores at the application sites for each treatment group and experimental time point, and indicating the degree of skin irritation on a scale ranging from 0.0 (negligible irritation) to 8.0 (severe irritation), are shown in Fig. 5a. According to the response categories defined in ISO 10993-23 (2021), the PII scores for *GGMA nanocomp* and CTR- groups indicate that the irritation responses were negligible, in contrast to the severe irritation response caused by SDS (CTR+).

3.6.2. Delayed-type hypersensitivity test

After forty-eight hours from patch removal, no signs of erythema or oedema, hallmarks of cell-mediated hypersensitivity reactions, were observed in either female or male animals treated with *GGMA nanocomp*, nor in the negative controls. By contrast, seven out of ten guinea pigs (four females and three males) treated with α-hexylcinnamaldehyde (a known sensitizer) showed patchy to confluent erythema. Therefore, the sensitisation rate for the CTR– and *GGMA nanocomp*-treated groups

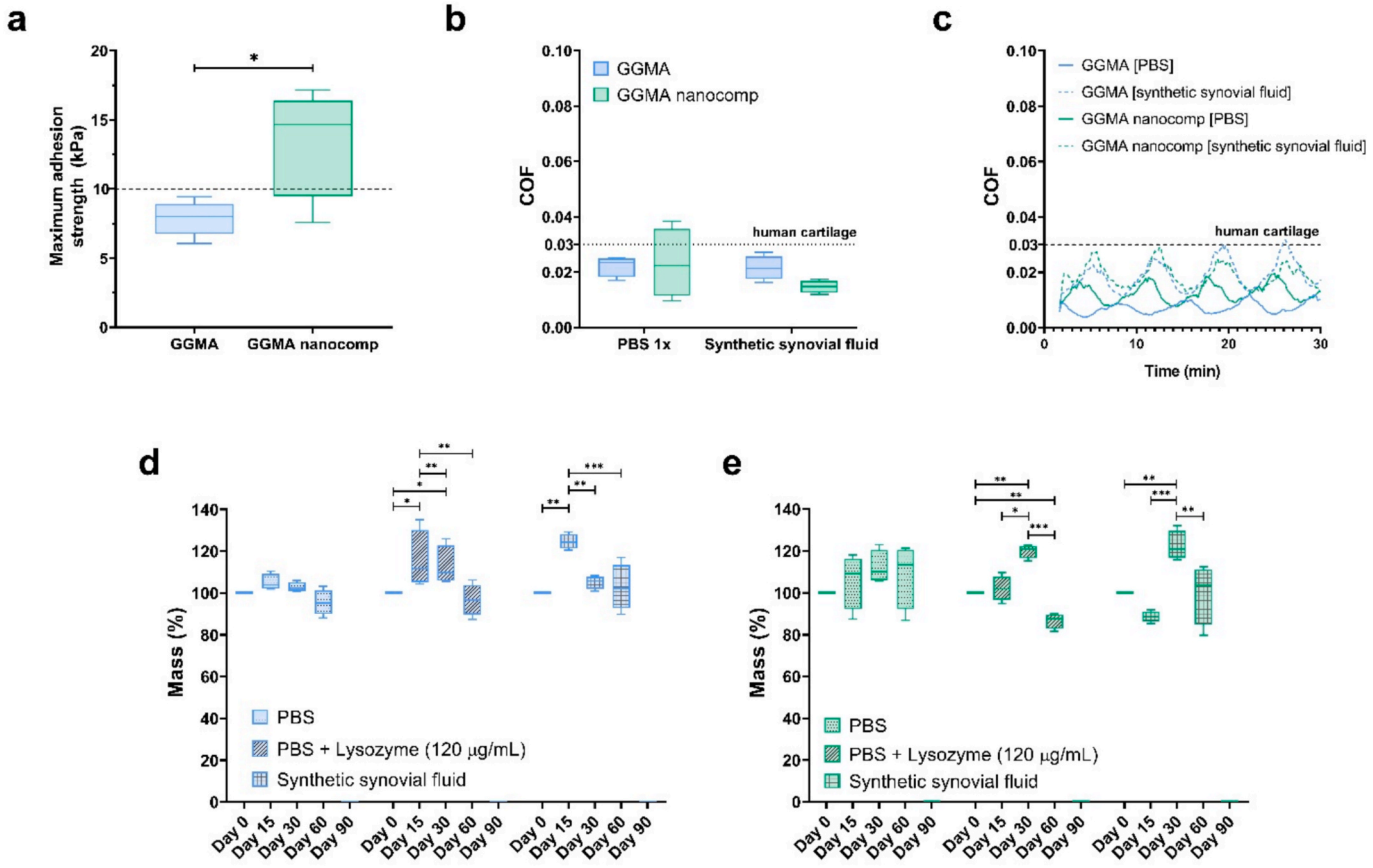

Fig. 3. Characterization of photo-crosslinked GGMA and GGMA nanocomp. a) Maximum adhesion strength between the hydrogel and the cartilage sample calculated during the tension tests (n = 5). The dashed line indicates the clinically compatible adhesion strength to the cartilage equal to 10 kPa [49]. Data in a) were presented as box plots, displaying the median, minimum, and maximum values; Mann−Whitney U-test, *p < 0.05. b) Coefficient of friction (COF) evaluated varying the sliding speed 10^{-5} to 102 min^{-1} under a constant 0.5 N load in PBS and ISO 14243-compliant synthetic synovial fluid (n = 4). c) COFs evaluated at a constant sliding speed of 5 min^{-1} for 30 min in PBS and ISO 14243-compliant synthetic synovial fluid. The dashed line in b) and c) evidences the human cartilage's COF equal to 0.03 [50]. d) and e) reported the degradation analysis of GGMA and GGMA nanocomp, respectively, up to 90 days (n = 4) in PBS, PBS+ Lysozyme (120 µg/mL), and ISO 14243-compliant synthetic synovial fluid environments. Data in b), d), and e) were presented as box plots, displaying the median, minimum, and maximum values; Kruskal−Wallis' test and the Dunn's multiple comparison test within groups; *p < 0.05; *p < 0.01; ***p < 0.001.

was 0%, and the *GGMA nanocomp* was classified as a weak sensitiser according to the Magnusson and Kligman classification (Fig. 5b). In contrast, the sensitisation rate for the CTR+ group was 70%, and the known sensitiser provoked strong sensitisation in the treated animals.

3.6.3. Acute and subchronic systemic toxicity

3.6.3.1. Acute systemic toxicity. The acute systemic toxicity test revealed no significant variations in body weight, water, or food consumption in the animals at 24-, 48-, or 72-hours post-treatment (Fig. 6a–c). No other signs of illness or adverse clinical symptoms were recorded at any time points.

3.6.3.2. Subchronic systemic toxicity. Statistical analysis of the body weights of male and female animals showed no difference between CTR– and *GGMA nanocomp* groups, as shown in Fig. 6d-e. In addition, no clinical symptoms were recorded at any time following *GGMA nanocomp* treatment. The investigation of the primary haematological parameters revealed a significant decrease in mean platelet volume (MPV) in both female and male animals and in plateletcrit (PCT) in males treated with *GGMA nanocomp* compared to their negative controls (Table 1 and Table 2).

Clinical biochemistry revealed a significant decrease in urea levels in both female and male G*GMA nanocomp*-treated rats (Fig. 7a-b). No other significant differences were found in biochemical parameters of *GGMA nanocomp*-treated female rats in comparison with CTR–ones (Fig. 7c). Furthermore, *GGMA nanocomp* male rats exhibited significantly higher levels of triglycerides and alkaline phosphatase (ALP) than CTR– rats (Fig. 7b-d). Urinalysis and serum protein electrophoresis analysis revealed no significant differences between *GGMA nanocomp* or CTR–treated rats (Supplementary Tables 4–6).

At necropsy, no macroscopic changes were observed. Representative microscopic images of the main explanted organs (brain, heart, liver, and kidney) from male and female *GGMA nanocomp* and CTR– groups, along with their corresponding weight measurements, are shown in Fig. 8a–d: they did not show histopathological alterations. A significant increase in liver weight was found in female rats treated with *GGMA nanocomp* compared with the CTR– group (Fig. 8c). Representative microscopic images of other organs (lung, spleen, thymus, uterus and ovary, testis and epididymus) are shown in the Supplementary Figs. 7 and 8 and similarly did not display any histopathological changes.

ICP-MS results, performed to identify titanium (Ti) and barium (Ba) residuals in blood and in the organs distant from the injection site, were reported in Supplementary Tables 7 and 8. Statistical analysis did not find significant differences in Ti and Ba levels between CTR– and *GGMA nanocomp*-treated females, while CTR– male animals exhibited significantly higher levels of Ba both in the brain and heart compared to *GGMA nanocomp*-treated ones.

3.6.3.3. Local effects after implantation. The semiquantitative scoring

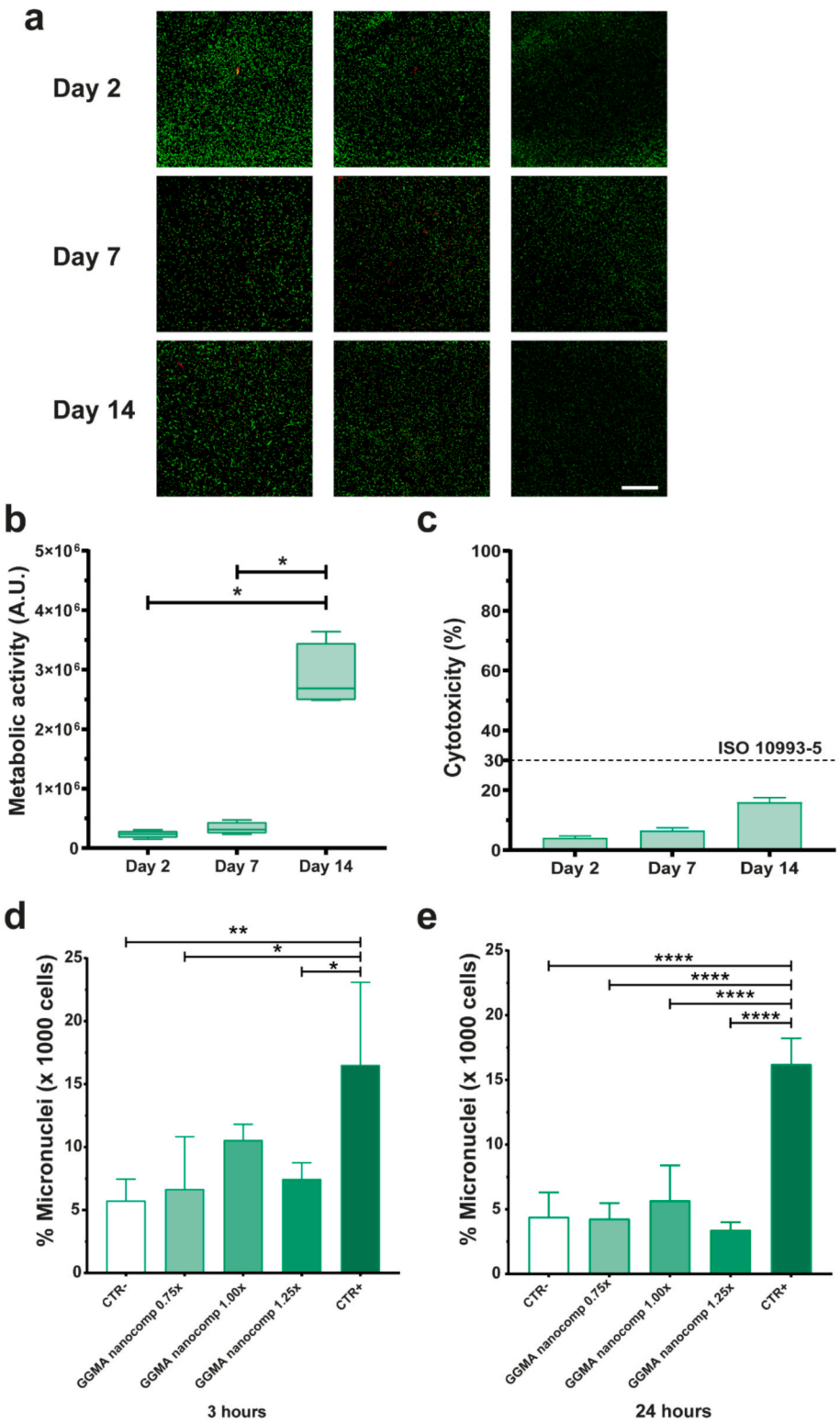

Fig. 4. Biological characterization of GGMA nanocomp embedding HCs after 2, 7, and 14 days and micronuclei test results. a) Cell viability (Live/Dead assay of three planes throughout the each hydrogel) (scale bar = 200 μm); b) metabolic activity (Presto blue assay; mean ± SD, Kruskal–Wallis' test and Dunn's multiple comparison test, n = 3), and c) cytotoxicity (LDH assay, box plots, displaying the median, minimum, and maximum values; Kruskal–Wallis' test and Dunn's multiple comparison test, n = 4) evaluated after 2, 7, and 14 days. The dashed line in (c) evidences the threshold in cytotoxicity in accordance with the ISO 10993-5 (2009) standard. d-e) Micronuclei frequencies (%) in TK6 cells exposed to three concentrations of GGMA nanocomp (GGMA nanocomp 075x, GGMA nanocomp 1x, GGMA nanocomp 1.25x), or negative control (CTR−, RPMI medium) and positive control (CTR+, 0.5 μg/mL H_2O_2), for 3 (d) and 24 (e) hours. Data are presented as mean ± SD. Two independent experiments were performed in duplicate. One-way ANOVA followed by a Sidak post hoc test (*$p < 0.05$, **$p < 0.01$, ***$p < 0.001$, ****$p < 0.0001$).

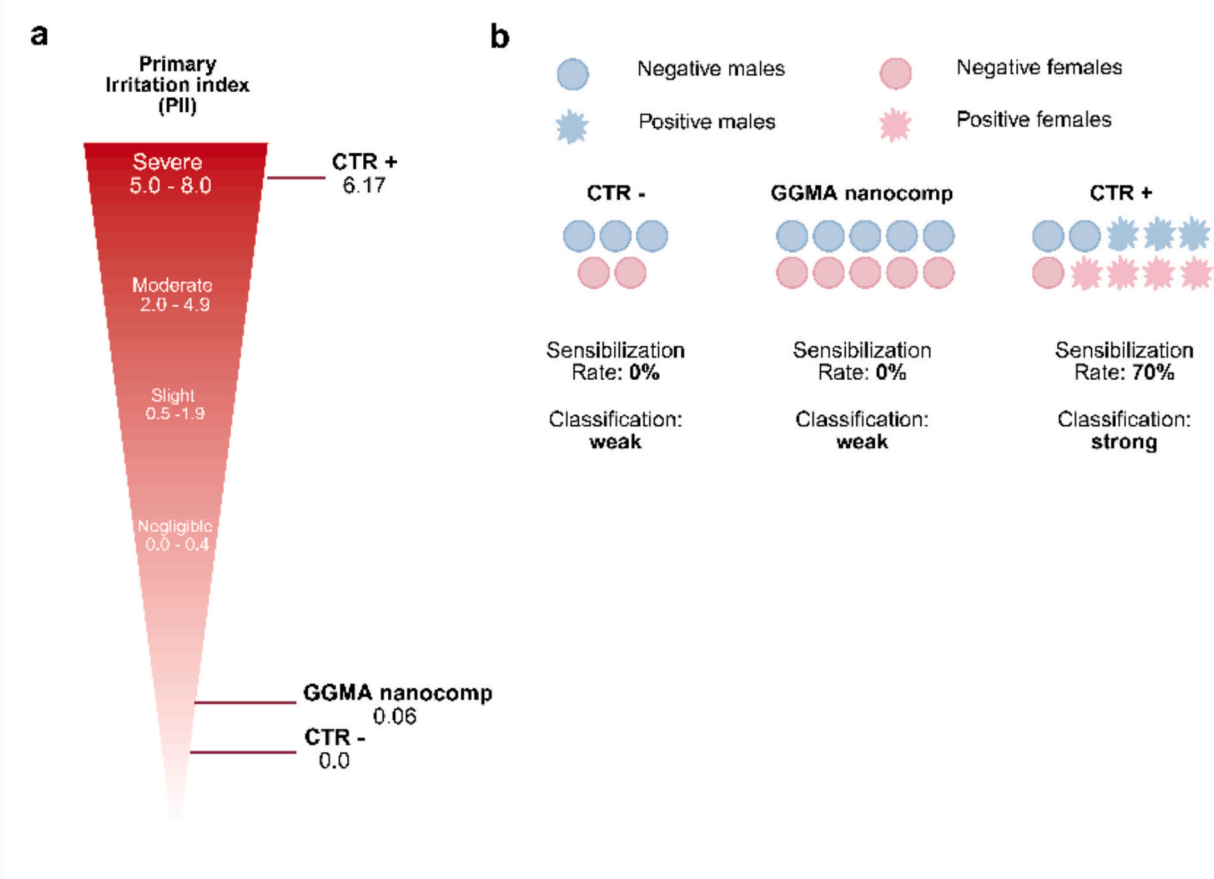

Fig. 5. Skin irritation and delayed-type hypersensitivity test results. Results of a) Primary irritation index from skin irritation test conducted on rabbits topically treated with GGMA nanocomp (n = 6), physiological saline solution (CTR−) (n = 6) and SDS (CTR+) (n = 4), b) skin sensitization rates and corresponding classifications based on the Magnusson and Kligman scale, as observed in male and female animals from each treatment group (GGMA nanocomp, CTR−, and CTR+).

system from Annex E, ISO 10993-6 (2016) was applied to histological images of female and male *GGMA nanocomp*- and Hymovis®-treated joints to obtain the reactivity ranking. In comparison with the clinical control Hymovis®, *GGMA nanocomp* was considered to demonstrate a slight reaction to the tissue. In addition, no significant microscopic differences were evidenced in synovial membranes and draining popliteal lymph nodes from *GGMA nanocomp*-treated animals in comparison with controlateral clinical control-treated ones (Fig. 9a-b). Similarly, no statistically significant differences were highlighted in WBC counts as an indicator of local inflammatory response in the synovial fluid of male and female animals treated with *GGMA nanocomp* when compared with clinical control Hymovis® (Fig. 9c-d).

4. Discussion

This study aimed to provide a comprehensive evaluation of the physicochemical properties and safety profile of a visible light-crosslinked nanocomposite hydrogel based on *GGMA* for cartilage treatment (Supplementary Table 1). The outcomes demonstrated that the inclusion of functional nanomaterials (BTNPs at 50 μg/mL and GO nanoflakes at 25 μg/mL) into the *GGMA* hydrogel enhances its rheological, mechanical, adhesive, and lubrication performance without compromising injectability, while showing no adverse effects on biocompatibility in both *in vitro* and *in vivo* tests. The selection of nanomaterial concentrations was guided by evidence from previous studies assessing cytotoxicity in contact with cells [38,53,54]. Consistently, in our previous work [27], GO nanoflakes and BTNPs were systematically incorporated into ionically crosslinked alginate-based hydrogels at different concentrations (10, 25, 50, and 100 μg/mL). That study demonstrated that GO nanoflake concentrations above 25 μg/mL induced a significant reduction in cell viability compared to control cells, whereas BTNPs exhibited good cytocompatibility up to 100 μg/mL. From the rheological perspective, the addition of BTNPs and GO to the *GGMA* led to a significant increase in the consistency index in both pre- and post-crosslinked states, without altering the shear-thinning behaviour of the hydrogel. In the pre-crosslinked state, nanomaterial-polymer interactions probably restricted polymer chain dynamics, resulting in increased viscosity. Nonetheless, the shear stress generated during the injection remained safely below the threshold considered harmful for cells (5 kPa) [55].

After photo-crosslinking, the incorporation of nanomaterials did not alter the overall network architecture of the hydrogels, as qualitatively confirmed by SEM imaging. The images showed a semi-porous surface of the hydrogel due to the lyophilization process [56], while open porosity was observed in both *GGMA* and *GGMA nanocomp* hydrogels when cut to visualize their cross-sections [57]. Despite the preserved morphology with the introduction of nanomaterials, a clear enhancement in network formation was observed in the nanocomposite system, as indicated by the reduced sol fraction values from 10.76 ± 1.31% for *GGMA* to 5.37 ± 2.22% for *GGMA nanocomp*. This behavior suggests an increased crosslinking efficiency, likely arising from the introduction of additional physical interaction points provided by the nanomaterials, which promote a denser and more interconnected polymer network. The impact of this reinforced structure was evident at the macroscopic level. GGMA-based hydrogels demonstrated a swelling behavior similar to our previous works [40], with *GGMA nanocomp* hydrogels displaying a significantly reduced swelling ratio over time. The reduced water uptake over time indicates a more stable and constrained network in the presence of

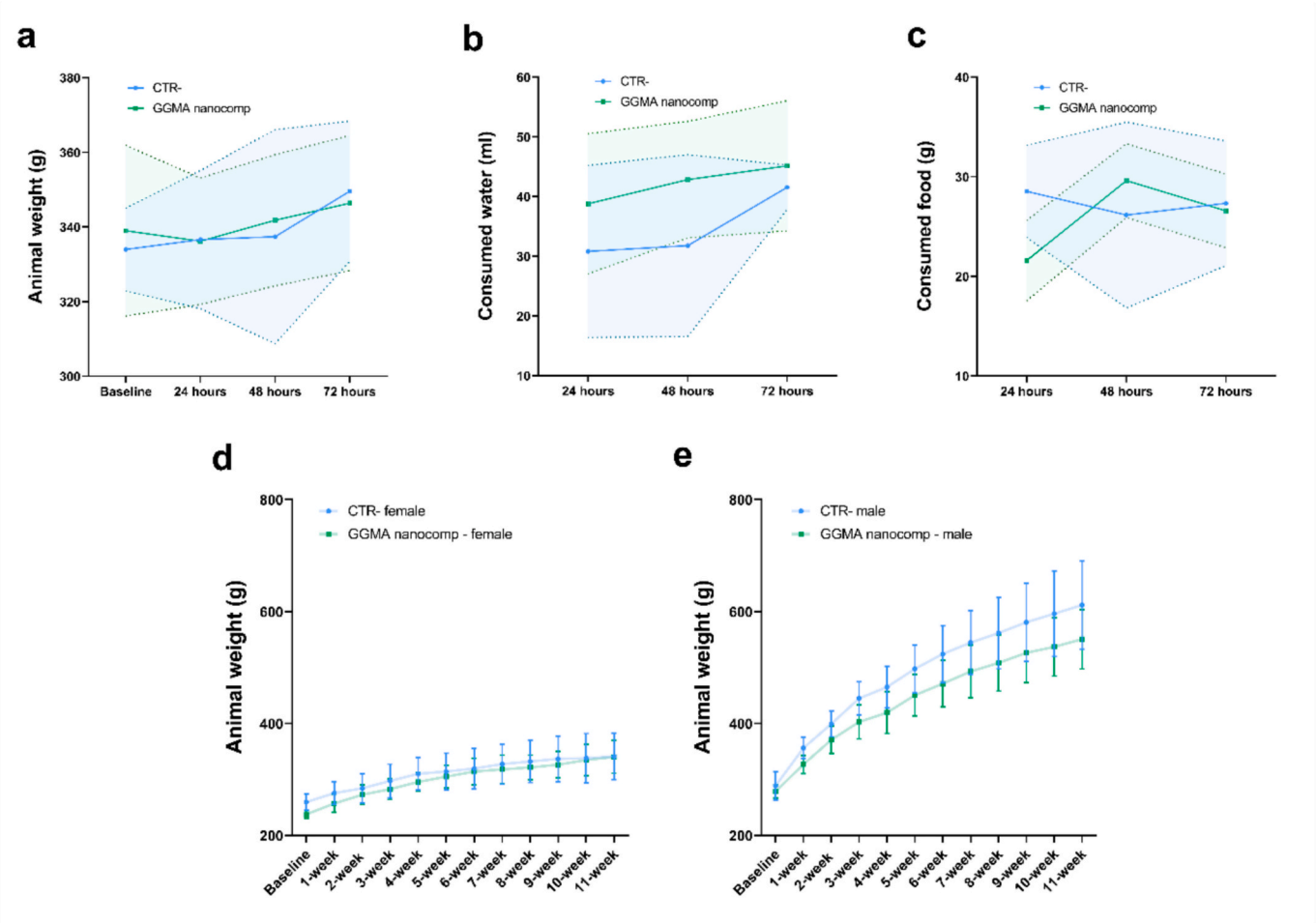

Fig. 6. Acute and subchronic systemic toxicity results. Results of the baseline measurements of a) body weight, b) water consumption, and c) food consumption, as well as the 24-, 48-, and 72-hour measurements following treatment with physiological saline solution or GGMA nanocomp during the acute systemic toxicity test performed on male rats (n = 5). Data are presented as mean (solid lines) ± SD (dashed lines). Body weight measurements of subchronic systemic toxicity in d) female (n = 10) and e) male (n = 10) rats intraarticularly treated to GGMA nanocomp and physiological saline solution. Data are represented as mean ± SD.

Table 1
Hematological values for female rats in the negative control (CTR−) and GGMA nanocomp groups.

Female Rats	CTR–	*GGMA nanocomp*	Reference range [51,52]
Hb g/dL	14.5 ± 0.3	14.3 ± 0.9	11.7-17.3
HCT %	40.8 ± 1.8	39.2 ± 2.3	35.2-49.8
RBC x 10^6/ml	7.4 ± 3.4	7.4 ± 7.0	6.3-9.3
MCV fL	55.0 ± 1.5	53.3 ± 2.7	48.8-59.5
MCH pg	19.5 ± 0.6	19.5 ± 1.1	16.5-19.8
MCHC g/L	354.6 ± 1.1	364.7 ± 0.4	322–367
MPV fL	8.8 ± 0.4	7.5 ± 0.4 **	6.7–8.1
WBC x 10^3/ml	7.0 ± 1.3	7.3 ± 2.9	2.9–17.7
Neutrophils%	10.4 ± 2.1	13.7 ± 2.4	5.2-28
Lymphocytes%	85.6 ± 2.7	82.6 ± 2.9	66.6-90.7
Monocytes%	2.2 ± 0.8	2.1 ± 0.4	1-6.1
Eosinophils%	1.0 ± 0.5	0.8 ± 0.4	0.6-5.9
Basophils%	0.2 ± 0.1	0.2 ± 0.1	0.0-0.6
Platelets 10^6/ml	1030 ± 140.1	901.8 ± 156	561-1377
PCT %	0.9 ± 0.1	0.7 ± 0.1	0.6–1.7

*Data are expressed as mean ± SD (n = 10). Student's test vs CTR– (**p < 0.01).*

Table 2
Hematological values for male rats in negative control (CTR−) and GGMA nanocomp groups.

Male Rats	CTR–	*GGMA nanocomp*	Reference range [51,52]
Hb g/dL	15.9 ± 1.0	15.6 ± 0.5	13.5-18.4
HCT %	44.4 ± 3.0	43.4 ± 0.8	38.9-54.9
RBC x 10^6/ml	8.5 ± 4.6	8.4 ± 2.7	7.8-10.2
MCV fL	52.1 ± 1.1	51.5 ± 0.9	45.5-60.8
MCH pg	18.7 ± 0.5	18.4 ± 0.3	15.7-19.7
MCHC g/L	358.3 ± 0.7	358.2 ± 0.8	316–358
MPV fL	9.1 ± 0.6	7.8 ± 0.2 **	6.7–8.1
WBC x 10^3/ml	10.9 ± 1.8	14.3 ± 4.3	5.9–19
Neutrophils%	16.7 ± 7.3	10.2 ± 3.2	5.3–45.1
Lymphocytes%	74.0 ± 18.8	86.1 ± 3.5	51.8-89.7
Monocytes%	7.5 ± 12.8	1.7 ± 0.4	1.3-6
Eosinophils%	1.0 ± 0.7	1.1 ± 0.5	0.5-7.2
Basophils%	0.3 ± 0.1	0.3 ± 0.1	0.0-0.6
Platelets 10^6/ml	878.86 ± 169.1	726.77 ± 83.3	529–1383
PCT %	0.8 ± 0.1	0.6 ± 0.1 **	0.6–1.7

Data are expressed as mean ± SD (n = 10). Student's t test vs CTR– (**p < 0.01). Hb = Haemoglobin; HCT = Haematocrit; RBC = Red Blood Cells; MCV = Mean Cell Volume; MCH = Mean Corpuscular Hemoglobin; MCHC = Mean Corpuscular Hemoglobin Concentration; MPV = Mean Platelet Volume; WBC = White Blood Cells; PCT = Plateletcrit.

nanomaterials [58]. In accordance with these results, the bulk mechanical properties were significantly improved, with the compressive modulus increasing from 0.89 ± 0.06 kPa for *GGMA* to 1.30 ± 0.17 kPa for *GGMA nanocomp*. These findings support a filler-mediated network constraint effect, in which nanofiller–polymer interactions limit chain mobility and enhance mechanical stiffness [59]. Importantly, these results also indicate that the visible light–mediated polymerization

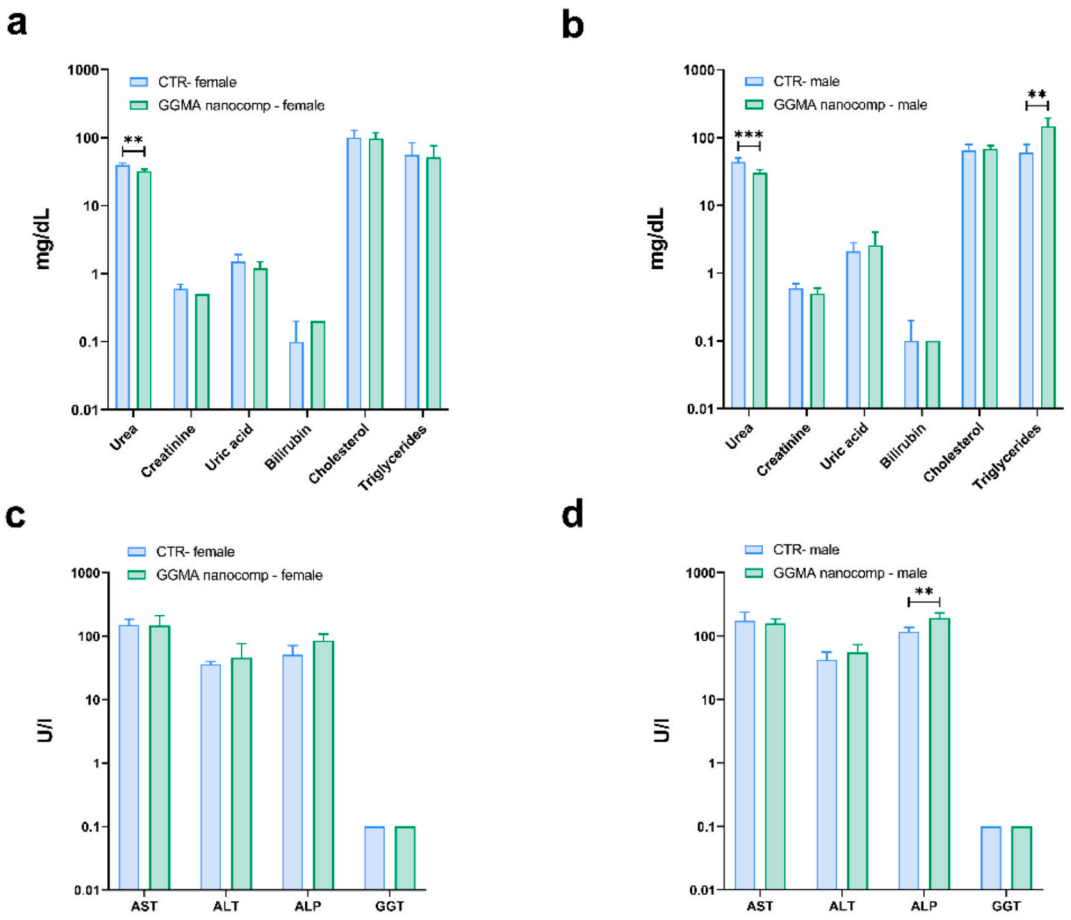

Fig. 7. Subchronic systemic toxicity results. Main biochemical parameters measured in the blood of female (a, c) and male (b, d) animals of negative control group (CTR–) and the GGMA nanocomp ones. The Y-axis is shown on a logarithmic scale (log10) to allow visualization of values spanning a wide range. Data are presented as mean ± SD (n = 10). Student's t-test vs. CTR– (**p < 0.01, ***p < 0.001). AST = Aspartate Aminotransferase; ALT = Alanine Aminotransferase; ALP = Alkaline Phosphatase; GGT = Gamma-glutamyl transferase.

process remained effective in the presence of nanofillers, which did not significantly interfere with light absorption in the relevant spectral range, as evidenced by the increased crosslinking efficiency and improved mechanical performance. This aspect is particularly relevant, as the incorporation of nanomaterials into photo-crosslinkable hydrogels often poses challenges due to potential light attenuation, which can necessitate longer exposure times and ultimately compromise crosslinking efficiency [60]. As previously reported [27], the mechanical reinforcement provided by these nanomaterials was observed in ionically crosslinked hydrogels, a purely physical approach that does not involve external irradiation. In this work, visible-light photo-crosslinking was successfully conducted to get a nanocomposite hydrogel, since both BTNPs and GO preferentially absorb at the lower end of the visible spectrum and in the UV range [61,62]. Overall, the mechanical data demonstrate that the presence of nanomaterials enhances the compressive modulus of visible-light–crosslinked GGMA hydrogels, at a relatively low nanofiller concentration.

The *GGMA nanocomp* exhibited stronger adhesive performance on cartilage tissue compared to *GGMA* alone, exceeding the 10 kPa clinical benchmark [49]. The enhancement in adhesion strength observed for *GGMA nanocomp* (13.28 ± 3.81 kPa) compared to pristine *GGMA* (7.87 ± 1.25 kPa) (Fig. 3a) can be interpreted within a multi-mechanism adhesion framework acting at the interface. The methacrylated groups in *GGMA* can primarily form covalent bonds with free amine, thiol, or hydroxyl groups naturally present in tissue proteins, enabling effective anchoring of the hydrogel at the tissue interface during the photo-crosslinking phase. In parallel, non-covalent interactions such as hydrogen bonding and electrostatic interactions with glycosaminoglycans and collagen, further contribute to interfacial stability, likely attributed to the presence of additional adhesion sites on cartilage [63]. The incorporation of GO and BTNPs results in an approximately 70% increase in adhesion strength, which can be attributed to nanofiller-mediated interfacial reinforcement mechanisms. These include an increase in effective contact area and surface roughness, the introduction of additional interaction sites, and improved stress distribution at the interface. In particular, GO nanoflakes introduce oxygen-containing functional groups that can establish additional hydrogen bonding and promote protein adsorption at the interface, thereby increasing the density of secondary interactions with the cartilage surface [64]. These combined effects explain the observed increase in adhesion strength in the nanocomposite formulation from sub-clinical adhesion values in *GGMA* to values exceeding the clinically relevant threshold of 10 kPa in *GGMA nanocomp*. This result is consistent with previous observations in ionically crosslinked, alginate-based hydrogels, where GO concentrations ≥ 25 μg/mL produced a comparable adhesion-enhancing effect [27], indicating a consistent behaviour across different hydrogel systems. The use of GO at 25 μg/mL provides an optimal balance between biological safety and adhesion performance. The *GGMA nanocomp* also exhibited a notable ability to be retained on cartilage tissue upon deposition. For potential *in situ* delivery on the cartilage surface, it was observed that the material remained stably attached at all orientations except at 90° and 135°. Notably, these findings indicated that the inclusion of nanomaterials within the *GGMA* can promote hydrogel adhesion after injection and polymerization at the target site,

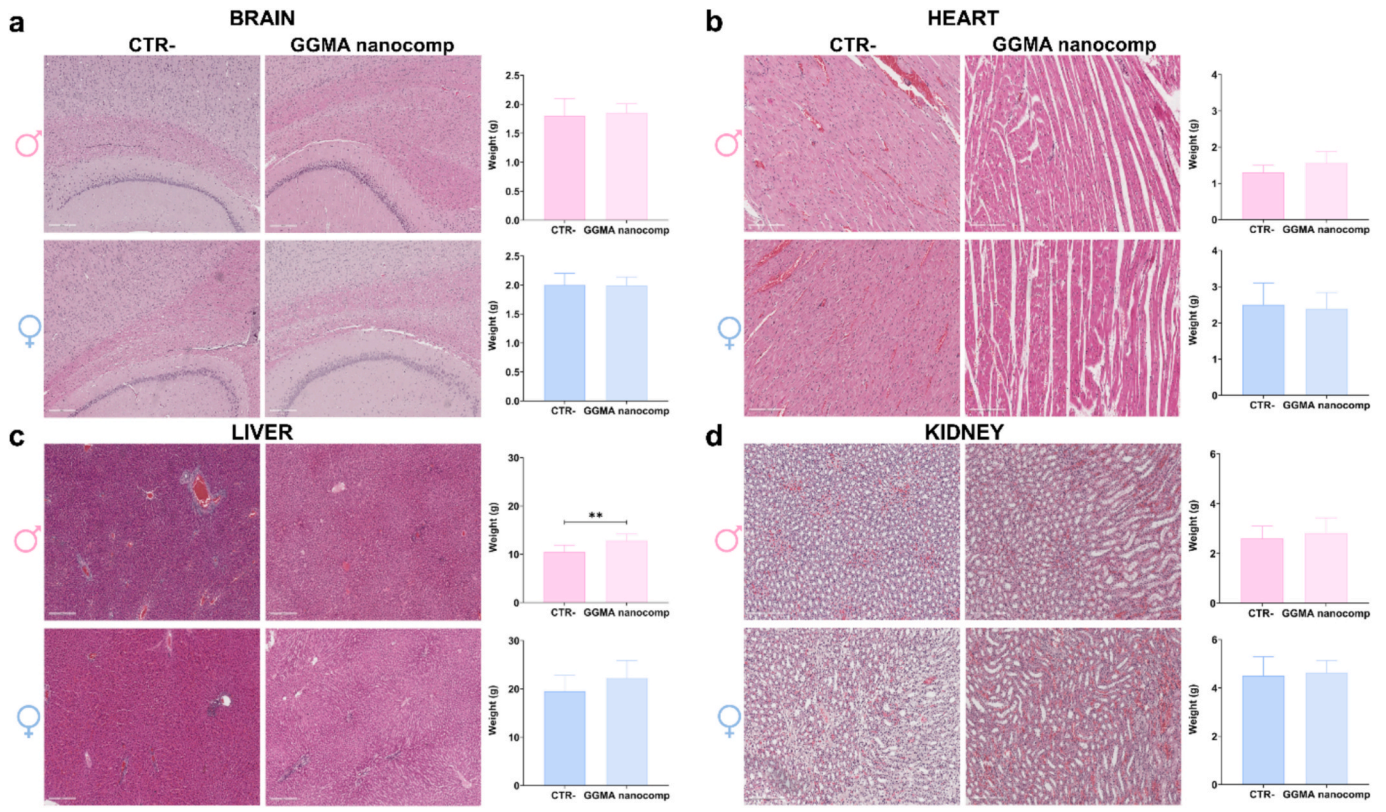

Fig. 8. Subchronic systemic toxicity results. Representative haematoxylin and eosin (H&E)-stained images of the (a) brain (20x magnification, bar = 300 μm), (b) heart (20x magnification, bar = 200 μm), (c) liver (20x magnification, bar = 300 μm) and (d) kidney (20x magnification, bar = 200 μm) from female and male rats treated with GGMA nanocomp (right panels) or the control group (left panels). Bar graphs show organ weights at explant according to sex and treatment group. Data are presented as mean ± SD (n = 10). Student's t-test vs. CTR– (**$p < 0.01$).

eliminating the need for primers to mediate attachment to tissue [40].

Then, since lubrication is a key functional property of articular cartilage, the COF of the hydrogels was measured to assess the effect of nanomaterial incorporation on *GGMA*'s lubrication performance. The COF in both *GGMA* and *GGMA nanocomp* remained within the physiological range (0.001–0.03) [50] in PBS and synthetic synovial fluid, with no significant variation over 30 minutes of testing. Wear tests confirmed that both hydrogels withstand continuous mechanical loading without dramatically altering surface lubrication properties. Since *GGMA* already exhibited favourable lubrication properties (COF < 0.03), the inclusion of nanomaterials did not provide additional benefit in this respect. Degradation studies showed no marked mass loss in either formulation under any tested condition. Specifically, GGMA-based hydrogels remained relatively stable in both PBS and ISO 14243-compliant synthetic synovial fluid, which reproduce physiological buffering conditions and joint-like rheological environments, respectively. The limited degradation observed in synthetic synovial fluid is consistent with the fact that this medium mimicked only the rheological properties of native synovial fluid and did not recapitulate the full biological and enzymatic complexity of pathological joint environments. In contrast, both *GGMA* and *GGMA nanocomp* hydrogels exhibited an early and significant degradation in the presence of lysozyme, an enzyme naturally found in synovial fluid under both physiological and inflammatory conditions as part of the innate immune response [65]. *GGMA* may degrade through both hydrolytic and enzymatic pathways, with hydrolysis of the methacrylate-derived ester bonds being the predominant mechanism, and enzymatic cleavage by glycosidases or esterases contributing to a lesser extent. The limited degradation observed here up to 60 days can likely be attributed to the efficient crosslink density of both *GGMA* and *GGMA nanocomp* [21], supporting their potential use in long-term cartilage applications where preservation of initial properties is critical. Notably, complete degradation of all samples was observed by 90 days across all tested conditions.

In the context of growing research on nanocomposite hydrogels for AC, the biocompatibility and assessment of local and systemic safety are pivotal criteria for implantable materials. For biomaterials and medical devices intended for use in the human body, ISO 10993 provides an internationally recognized guidance for biological evaluation within a risk-management framework. The developed *GGMA*-based hydrogel, classified as an implantable device intended for long-term contact with the musculoskeletal system, therefore requires an extensive panel of in vitro and in vivo tests prior to clinical translation. *In vitro* tests showed that human chondrocytes encapsulated in the *GGMA nanocomp* maintained high viability and increasing metabolic activity for up to 14 days, with cytotoxicity levels remaining below 30%, thus within the acceptance threshold defined by ISO 10993-5 (2009) [66,67]. Additionally, no statistically significant differences were found when compared with the previously published data on *GGMA* at the corresponding time point, indicating that nanomaterial incorporation did not introduce detectable adverse effects [21]. These results supported subsequent *in vivo* evaluations of the *GGMA nanocomp* for potential clinical applications in cartilage [10].

The results of the *in vitro* genotoxicity tests conducted in accordance with ISO 10993-3 (2014), including the Ames test on bacterial strains and the micronucleus test in a human lymphoblastoid cell line, confirmed the absence of genotoxic effects of *GGMA nanocomp*. The use of different test systems, such as an integrated platform combining bacterial and mammalian cells, is intended to provide a comprehensive evaluation of genotoxic potential: Ames's test excludes point mutations, and the micronuclei test the DNA damage. These findings from the Ames and micronucleus assays of the *GGMA nanocomp* are in line with existing literature. Previous studies showed that other inorganic ceramic-based

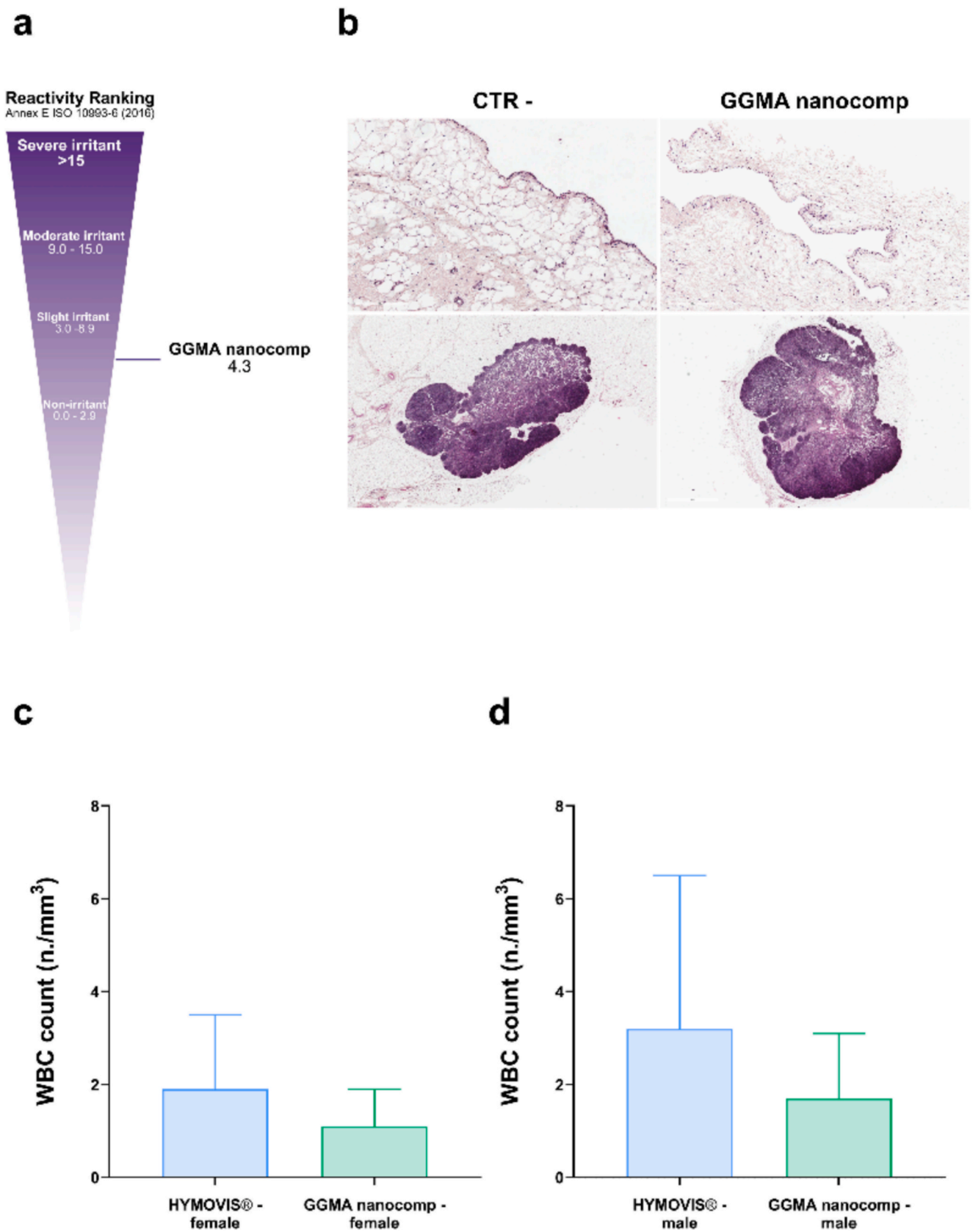

Fig. 9. Local effects after implantation results. a) Results of the semiquantitative scoring system for cellular and tissue responses after implantation in female and male animals treated with Hymovis® or with GGMA nanocomp. Data are expressed as mean ± SD (n = 5); b) Representative histological images of the synovial membranes (20x magnification, bar = 200 μm) and the draining popliteal lymph nodes (4x magnification, bar = 2mm) of GGMA nanocomp- (upper and lower left, respectively) and Hymovis® (upper and lower right, respectively)-treated knee joints. Haematoxylin-Eosin staining. WBC counts in synovial fluid of c) female and d) male treated with Hymovis® and with GGMA nanocomp. Data are expressed as mean ± SD (n = 5).

nanoparticles did not generate a genotoxic response when tested at different concentrations on human cell lines. Instead, the genotoxicity of graphene-based materials for biomedical applications, such as GO nanoflakes as those incorporated in *GGMA nanocomp*, has also been examined through a battery of *in vitro* tests, such as the micronucleus and comet assays, on immortalised mammalian cell lines [68–71].

After proving *in vitro* the absence of cytotoxicity and genotoxicity of *GGMA nanocomp,* the *in vivo* safety and biocompatibility were assessed through skin irritation, delayed-type hypersensitivity, acute and sub-chronic systemic toxicity, and local effects after implantation tests. Skin irritation, delayed-type hypersensitivity and systemic acute toxicity were carried out to evaluate short-term adverse effects after contact with the nanocomposite hydrogel in comparison with appropriate negative and positive controls. The *GGMA nanocomp*-treated group exhibited a favourable skin and immunological tolerability profile, as evidenced by its low PII in the skin irritation test and the absence of allergic reactions upon contact in GPMT. The results of the acute systemic toxicity test confirmed the biocompatibility of the *GGMA nanocomp* compared to non-exposed controls. No significant changes in body weight, food and water intake, or clinical signs were observed within 72 hours after the end of treatment, suggesting that *GGMA nanocomp* did not induce acute systemic toxic effects.

In the subchronic systemic toxicity study, both male and female rats treated with the *GGMA nanocomp* or control physiological saline (CTR–), exhibited a physiological increase in body weight and showed no observable clinical signs of toxicity. However, a significant decrease in the mean platelet volume (MPV), an indicator of platelet size, was observed in *GGMA nanocomp*-treated female and male rats; however, MPV values remained within their reference ranges. This finding was not supported by changes in platelet count in females and males in both treatment groups. Therefore, this variation could be attributed to technical variability and to age-related increase in MPV in animal models, as well as in humans [72], due to the physiological ageing of platelets, as reported in the study of Patel *et al.* in Wistar rats [73]. Furthermore, mean corpuscular haemoglobin concentration (MCHC) values of CTR– and *GGMA nanocomp* male rats were slightly above the upper limit of the reference range [51]. However, the similarity in both groups suggested that this increase could be attributable to intrinsic biological variability. Finally, PCT values were significantly lower in males treated with *GGMA nanocomp* than in the control group (CTR–) but remained within their physiological ranges [74]. In the subchronic systemic toxicity study, both male and female rats treated with the *GGMA nanocomp* or control physiological saline (CTR–), exhibited a physiological increase in body weight and showed no observable clinical signs of toxicity. However, a significant decrease in the mean platelet volume (MPV), an indicator of platelet size, was observed in *GGMA nanocomp*-treated female and male rats, while remaining within their reference ranges. This finding was not supported by changes in platelet count in females and males in both treatment groups. Therefore, this variation could be attributed to technical variability and to age-related increase in MPV reported in both animal models and humans [72], due to the physiological ageing of platelets, as reported in the study of Patel *et al.* in Wistar rats [73]. In the biochemical panel, blood urea, a marker of kidney function, was significantly higher in CTR– female and male animals than in *GGMA nanocomp*-treated rats in both sexes, with CTR- values exceeding the reference ranges (female: 11–17 mg/dL; male: 10–16 mg/dL) [52]. Data from the literature show that, as in humans, a deterioration in kidney function is observed in animals with increasing age.

Finally, a significant increase in alkaline phosphatase (ALP) and triglyceride levels was observed in males treated with *GGMA nanocomp* compared to the control group. These values were outside the sex-based reference range (ALP – male: 140–160 U/L; Triglycerides – male: 62–92 mg/dL) [52]. Patlolla et al. reported that the oral administration of GO to adult male Sprague-Dawley rats increased ALP liver enzyme levels and caused histopathological alterations, showing dose-dependent hepatic effects such as hepatocyte disruption, hepatocellular vacuolation, pyknosis, hepatocyte karyomegaly, and liver atrophy [75]. In the present study, the increase in ALP was not accompanied by an increase in other biochemical parameters or by histopathological alterations. The observed increase in ALP may be related to a mild and transient systemic inflammatory response and local reactions at the joint level following intra-articular injection of the *GGMA nanocomp*. This hypothesis was supported by the fact that alkaline phosphatase (ALP) is not exclusively expressed by hepatocytes, but is also produced by osteoblasts and chondrocytes, where it plays a key role in bone and cartilage metabolism [76,77].

Similarly, the significant increase in triglycerides observed in *GGMA nanocomp*-treated males compared to CTR– ones was not linked to histopathological liver changes, but it could reflect a hormonal modulation of lipid metabolism. Also, a previous work of Mohammadkhani *et al.* demonstrated via metabolomic analysis that orally administration of GO nanosheets caused a significant decrease in steroid hormone biosynthesis, including testosterone [78]. According to the literature, GO nanoflakes in *GGMA nanocomp* might have reduced testosterone levels, impairing lipid clearance or increasing triglyceride synthesis. However, further insights are required for this mechanism, as the hormone's levels were not measured in this study. The rise in triglyceride levels and liver weight seen in urea could also be explained by the natural ageing process.

Nevertheless, macroscopic analyses at necropsy revealed no gross alterations in female or male rats from the CTR– or *GGMA nanocomp* groups. *GGMA nanocomp*-treated females exhibited a statistically significant increase in liver weight compared to controls, in the absence of histopathological and clinical alterations. This finding was not considered indicative of hepatic toxicity, since the ratio between liver weight and body weight remained within the reported physiological ranges (2–4%/BW) [79]. The absence of histopathological and clinical anomalies, together with only isolated haematological and biochemical changes, indicates that *GGMA nanocomp* is not systemically toxic. This conclusion is further supported by ICP-MS analysis, which confirmed that no Ba or Ti residues were detected in distant organs.

Lastly, the local effects resulting from the implantation test were evaluated using the semi-quantitative scoring system outlined in Annex E, in accordance with ISO 10993-6 (2016). This scoring system, applied to histological sections of synovial membranes from joints treated with the control clinically used Hymovis® (CTR−) and *GGMA nanocomp* in both male and female rabbits, evaluates inflammatory cellular and tissue parameters such as neovascularization, fibrosis, necrosis, and fatty acid infiltration. The results indicated that the *GGMA nanocomp* induced only a slight local reaction, which was further supported by the absence of histopathological alterations in the draining popliteal lymph nodes, as well as comparable white blood cell counts in the synovial fluid. This local response suggested a favourable local tolerability of the material when implanted intra-articularly, supporting its potential use in cartilage applications.

Numerous studies in the literature have explored the potential of innovative nanocomposite hydrogels for the treatment of cartilage lesions and OA, thanks to high biocompatibility and controllable degradation times [80–87]. These nanomaterial-enriched hydrogels have been shown both *in vitro* and *in vivo* to be free of cytotoxicity and inflammation, and to stimulate chondrogenesis. However, these studies have focused on characterization and efficacy evaluations rather than safety assessments or without the application of international ISO guidelines. This makes the comparison of materials with similar compositions.

Thus, the present work provides a comprehensive assessment of the nanocomposite hydrogel and its safety by complying with the relevant international standards (see Supplementary Table 1). This regulatory-compliant approach represents a fundamental step towards clinical applications. Future studies will be mandatory to evaluate the efficacy and the regenerative potential both *in vitro* and *in vivo*, to complete the translational nature of the research. In these efficacy studies, longer

experimental times and tracking studies might be adopted to confirm the presented safety studies here, in particular regarding the nanomaterial clearance and fate, and indirect effects on distant organs.

The major strength of our study was the strict adherence to ISO standards and regulatory compliance with a comprehensive battery of biocompatibility tests, which, by ruling out any toxicity concerns, significantly enhanced its translational potential, independently of the recipient's sex. Also, the selection of GO and BTNPs was guided by a multifunctional design principle, aiming to combine complementary contributions within a single hydrogel system. While GO primarily enhances mechanical properties, adhesion, and interfacial interactions, BTNPs provide an additional reinforcing effect on mechanical and adhesion properties and, importantly, introduce a piezoelectric component that may enable electromechanical coupling under physiological loading conditions, as suggested by the analysis with PFM (Supplementary Fig. S2). Although the concentration of nanomaterials was lower than in other studies investigating composite hydrogels [88–90], their integration into *GGMA* played a relevant role in enhancing the material's performance. Despite not being specifically examined in the present work, potential interactions between GO and BTNPs may occur through electrostatic and/or surface-mediated mechanisms, which could synergistically contribute to network reinforcement and enhanced adhesive properties; the extent and nature of this synergy will be further investigated in a dedicated follow-up study. Altogether, these findings positioned the *GGMA nanocomp* as a promising, injectable, mechanically responsive, and bioactive hydrogel for intra-articular applications and motivate the following *in vivo* validation.

Large-scale translation of *GGMA nanocomp* will require compliance with Good Manufacturing Practice (GMP) standards to ensure sterile, standardized, and reproducible production, guaranteeing batch-to-batch consistency, homogeneous nanomaterial dispersion, and *ad hoc* photopolymerization equipment and standardized light parameters for treating the joint space [91–94]. Moreover, the industrial scale-up also involves packaging, commercialization, and a deep analysis of the cost/benefit ratio, leading to high production costs.

Although current and adopted treatments like platelet-rich plasma (PRP) and hyaluronic acid formulations are widely used and clinically available at lower costs, their benefits can be variable and often require repeated administrations [95,96]. If long-term regenerative efficacy is confirmed, *GGMA nanocomp* may offer a combined mechanical support and regenerative stimulation, potentially reducing repeated interventions and long-term healthcare utilization.

5. Conclusion

This study presents a visible-light crosslinked nanocomposite methacrylated gellan gum (GGMA) hydrogel enriched with barium titanate nanoparticles (BTNPs) and graphene oxide (GO) nanoflakes for cartilage tissue. The nanocomposite formulation (*GGMA nanocomp*) demonstrated improved rheological, mechanical, and adhesive properties with respect to *GGMA* alone, while preserving lubrication and degradation profiles consistent with the clinical targets. Importantly, *GGMA nanocomp* exhibited a favourable biocompatibility profile under both systemic and local exposure conditions, with no evidence of cytotoxicity, genotoxicity, irritation, sensitization, systemic toxicity, or local inflammatory responses. The *in vivo* safety profile was evaluated in both male and female subjects, showing that the nanocomposite material did not exhibit evident adverse effects in either animal sex. These findings highlight the potential of GGMA-based nanocomposite hydrogels as safe and functional candidates for cartilage tissue applications. The combined *in vitro* performance and *in vivo* safety evidence establish a solid platform for translational advancement. Future studies will focus on evaluating regenerative efficacy on pathological chondrocytes and in preclinical models of focal articular cartilage lesions and post-traumatic osteoarthritis, paving the way toward clinical application.

CRediT authorship contribution statement

Giorgia Codispoti: Writing – review & editing, Writing – original draft, Visualization, Investigation, Data curation, Conceptualization. **Diego Trucco:** Writing – review & editing, Writing – original draft, Data curation, Conceptualization. **Melania Carniato:** Writing – original draft, Visualization, Investigation, Data curation. **Lorenzo Vannozzi:** Writing – review & editing, Visualization. **Lucia Martini:** Writing – review & editing, Supervision, Data curation. **Cristina Manferdini:** Writing – review & editing, Visualization. **Gina Lisignoli:** Writing – review & editing. **Matilde Tschon:** Writing – review & editing, Validation, Supervision, Resources, Data curation, Conceptualization. **Milena Fini:** Writing – review & editing. **Leonardo Ricotti:** Writing – review & editing, Supervision, Resources.

Funding

This work was supported by the European Union's Horizon 2020 research and innovation program, grant agreement No 814413, project ADMAIORA (*ADvanced nanocomposite MAterIals fOr in situ treatment and ultRAsound-mediated management of osteoarthritis*). We also acknowledge the support of the BRIEF "*Biorobotics Research and Innovation Engineering Facilities*" (project identification code IR0000036), project funded under the National Recovery and Resilience Plan (NRRP), Mission 4 Component 2 Investment 3.1 of the Italian Ministry of University and Research, funded by the European Union – NextGenerationEU.

Declaration of competing interest

The authors declare that they have no known competing financial interests or personal relationships that could have appeared to influence the work reported in this paper.

Acknowledgements

We acknowledge Dr. Jost and Dr. Fedutik for supplying us with BTNPs; Dr. Teblum, Dr. Telkhozhayeva, and Dr. Nessim for providing the GO nanoflakes; Mr. Fota, Fergnani, Pellini, Mrs. Samoggia, and Bonanno for their technical assistance; Dr. Fedrizzi and Prof. Dondi for ICP-MS and haemato-chemical and urine analyses, respectively.

Appendix A. Supplementary materials

Supplementary materials to this article can be found online at https://doi.org/10.1016/j.matdes.2026.116244.

Data availability

Data will be made available on request.

References

[1] K.L. Spiller, S.A. Maher, A.M. Lowman, Hydrogels for the repair of articular cartilage defects, Tissue Eng. Part B Rev. 17 (4) (2011) 281–299.
[2] S.U. Rehman, A.L. Malik, M.S. Jahangir, S. Iqbal, M.U. Shahid, Cartilage: Structure, Function, and the Pathogenesis of Osteoarthritis, in: A.R. Zorzi (Ed.), Advancements in Synovial Joint Science - Structure, Function, and Beyond, IntechOpen, Rijeka, 2024.
[3] M.B. Goldring, S.R. Goldring, Articular cartilage and subchondral bone in the pathogenesis of osteoarthritis, Ann. N. Y. Acad. Sci. 1192 (2010) 230–237.
[4] S.a. Tang, C. Zhang, W.M. Oo, K. Fu, M.A. Risberg, S.M. Bierma-Zeinstra, T. Neogi, I. Atukorala, A.-M. Malfait, C. Ding, D.J. Hunter, Osteoarthritis, Nature Reviews Disease Primers 11(1) (2025) 10.
[5] A. Mobasheri, R. Loeser, Clinical phenotypes, molecular endotypes and theratypes in OA therapeutic development, Nat. Rev. Rheumatol. 20 (9) (2024) 525–526.
[6] B. Cong, T. Sun, Y. Zhao, M. Chen, Current and novel therapeutics for articular cartilage repair and regeneration, Ther. Clin. Risk Manag. 19 (2023) 485–502.
[7] S. Grässel, D. Muschter, Recent advances in the treatment of osteoarthritis [version 1; peer review: 3 approved], F1000Research 9(325) (2020).

[8] D.J. Hunter, S. Bierma-Zeinstra, Osteoarthritis, Lancet (London, England) 393 (10182) (2019) 1745-1759.
[9] G. Merkely, J. Ackermann, C. Lattermann, Articular cartilage defects: incidence, diagnosis, and natural history, Operat. Tech. Sports Med. 26 (3) (2018) 156–161.
[10] Ø. Øvrebø, G. Perale, J.P. Wojciechowski, C. Echalier, J.R.T. Jeffers, M.M. Stevens, H.J. Haugen, F. Rossi, Design and clinical application of injectable hydrogels for musculoskeletal therapy, Bioeng. Transl. Med. 7 (2) (2022) e10295.
[11] D. Dehghan-Baniani, B. Mehrjou, P.K. Chu, W.Y.W. Lee, H. Wu, Recent advances in "functional engineering of articular cartilage zones by polymeric biomaterials mediated with physical, mechanical, and biological/chemical cues", Adv. Healthc. Mater. 12 (10) (2023) 2202581.
[12] C. Delbaldo, M. Tschon, L. Martini, M. Fini, G. Codispoti, Benefits of applying nanotechnologies to hydrogels in efficacy tests in osteoarthritis models-a systematic review of preclinical studies, Int. J. Mol. Sci. 23 (15) (2022).
[13] I.M. Oliveira, C. Gonçalves, M.E. Shin, S. Lee, R.L. Reis, G. Khang, J.M. Oliveira, Enzymatically crosslinked tyramine-gellan gum hydrogels as drug delivery system for rheumatoid arthritis treatment, Drug Deliv. Transl. Res. 11 (3) (2021) 1288–1300.
[14] J.T. Oliveira, L. Martins, R. Picciochi, P.B. Malafaya, R.A. Sousa, N.M. Neves, J. F. Mano, R.L. Reis, Gellan gum: a new biomaterial for cartilage tissue engineering applications, J. Biomed. Mater. Res. A 93A (3) (2010) 852–863.
[15] J.T. Oliveira, T.C. Santos, L. Martins, R. Picciochi, A.P. Marques, A.G. Castro, N. M. Neves, J.F. Mano, R.L. Reis, Gellan gum injectable hydrogels for cartilage tissue engineering applications: in vitro studies and preliminary in vivo evaluation, Tissue Eng. A 16 (1) (2010) 343–353.
[16] M.A. Bonifacio, A. Cochis, S. Cometa, A. Scalzone, P. Gentile, G. Procino, S. Milano, A.C. Scalia, L. Rimondini, E. De Giglio, Advances in cartilage repair: the influence of inorganic clays to improve mechanical and healing properties of antibacterial Gellan gum-Manuka honey hydrogels, Mater. Sci. Eng. C 108 (2020) 110444.
[17] A.H. Bacelar, J. Silva-Correia, J.M. Oliveira, R.L. Reis, Recent progress in gellan gum hydrogels provided by functionalization strategies, J. Mater. Chem. B 4 (37) (2016) 6164–6174.
[18] Z. Xu, Z. Li, S. Jiang, K.M. Bratlie, Chemically modified gellan gum hydrogels with tunable properties for use as tissue engineering scaffolds, ACS Omega 3 (6) (2018) 6998–7007.
[19] L.E. Agibayeva, D.B. Kaldybekov, N.N. Porfiryeva, V.R. Garipova, R. A. Mangazbayeva, R.I. Moustafine, I.I. Semina, G.A. Mun, S.E. Kudaibergenov, V. V. Khutoryanskiy, Gellan gum and its methacrylated derivatives as in situ gelling mucoadhesive formulations of pilocarpine: in vitro and in vivo studies, Int. J. Pharm. 577 (2020) 119093.
[20] J. Silva-Correia, B. Zavan, V. Vindigni, T.H. Silva, J.M. Oliveira, G. Abatangelo, R. L. Reis, Biocompatibility evaluation of ionic- and photo-crosslinked methacrylated gellan gum hydrogels: in vitro and in vivo study, Adv. Healthc. Mater. 2 (4) (2013) 568–575.
[21] D. Trucco, L. Vannozzi, E. Gabusi, E. Lenzi, C. Manferdini, A. Bacci, L. Agresti, M. R. Pascale, S. Cristino, G. Lisignoli, L. Ricotti, Visible light-mediated cross-linking of injectable gellan gum hydrogels embedding human chondrocytes, Carbohydr. Polym. Technol. Appl. 6 (2023) 100382.
[22] J. Jiang Luo, L. Rui Zhu, Z. Guo, N. Pi, X. Li, H. Lin Zou, H. Qun Luo, N. Bing Li, B. L. Li, Hydrogel-innovated nanotechnologies for chemical and biological analysis, Coord. Chem. Rev. 511 (2024) 215874.
[23] L. Liu, Z. Li, T. Zhu, Y. Sun, J. Xu, Advances in applications of low-dimensional piezoelectric materials in musculoskeletal system, Mater. Today Bio 33 (2025) 102065.
[24] A. Cafarelli, A. Marino, L. Vannozzi, J. Puigmartí-Luis, S. Pané, G. Ciofani, L. Ricotti, Piezoelectric nanomaterials activated by ultrasound: the pathway from discovery to future clinical adoption, ACS Nano 15 (7) (2021) 11066–11086.
[25] A. Sood, M. Desseigne, A. Dev, L. Maurizi, A. Kumar, N. Millot, S.S. Han, A comprehensive review on barium titanate nanoparticles as a persuasive piezoelectric material for biomedical applications: prospects and challenges, Small 19 (12) (2023) e2206401.
[26] L. Vannozzi, C. Pucci, D. Trucco, C. Turini, S. Sevim, S. Pané, L. Ricotti, Biodegradable piezoelectric micro- and nanomaterials for regenerative medicine, targeted therapy, and microrobotics, Small Sci. 5 (4) (2025) 2400439.
[27] L. Ricotti, A. Cafarelli, C. Manferdini, D. Trucco, L. Vannozzi, E. Gabusi, F. Fontana, P. Dolzani, Y. Saleh, E. Lenzi, M. Columbaro, M. Piazzi, J. Bertacchini, A. Aliperta, M. Cain, M. Gemmi, P. Parlanti, C. Jost, Y. Fedutik, G.D. Nessim, M. Telkhozhayeva, E. Teblum, E. Dumont, C. Delbaldo, G. Codispoti, L. Martini, M. Tschon, M. Fini, G. Lisignoli, Ultrasound stimulation of piezoelectric nanocomposite hydrogels boosts chondrogenic differentiation in vitro, in both a normal and inflammatory milieu, ACS Nano 18 (3) (2024) 2047–2065.
[28] C. Paci, F. Iberite, L. Arrico, L. Vannozzi, P. Parlanti, M. Gemmi, L. Ricotti, Piezoelectric nanocomposite bioink and ultrasound stimulation modulate early skeletal myogenesis, Biomater. Sci. 10 (18) (2022) 5265–5283.
[29] N. Parvin, V. Kumar, S.W. Joo, T.K. Mandal, Emerging trends in nanomedicine: carbon-based nanomaterials for healthcare, Nanomaterials (2024).
[30] D. Trucco, L. Vannozzi, E. Teblum, M. Telkhozhayeva, G.D. Nessim, S. Affatato, H. Al-Haddad, G. Lisignoli, L. Ricotti, Graphene Oxide-Doped Gellan Gum–PEGDA Bilayered Hydrogel Mimicking the Mechanical and Lubrication Properties of Articular Cartilage, Advanced Healthcare Materials n/a(n/a) (2021) 2001434.
[31] S. Affatato, D. Trucco, P. Taddei, L. Vannozzi, L. Ricotti, G.D. Nessim, G. Lisignoli, Wear behavior characterization of hydrogels constructs for cartilage tissue replacement, Materials 14 (2) (2021) 428.
[32] M. Zhou, N. Lozano, J.K. Wychowaniec, T. Hodgkinson, S.M. Richardson, K. Kostarelos, J.A. Hoyland, Graphene oxide: a growth factor delivery carrier to enhance chondrogenic differentiation of human mesenchymal stem cells in 3D hydrogels, Acta Biomater. 96 (2019) 271–280.
[33] M. Tschon, G. Codispoti, P. Cabras, A. Cafarelli, D. Trucco, L. Vannozzi, C. Manferdini, M. Carniato, G. Cassiolas, L. Martini, M. Fini, G. D'Atri, C. Jost, Y. Fedutik, G.D. Nessim, E. Dumont, G. Lisignoli, L. Ricotti, In vivo efficacy of an injectable piezoelectric nanocomposite hydrogel and low-intensity pulsed ultrasound in two preclinical models of osteoarthritis, Biomaterials 326 (2026) 123728.
[34] Z. Zheng, D. Eglin, M. Alini, G.R. Richards, L. Qin, Y. Lai, Visible light-induced 3D bioprinting technologies and corresponding bioink materials for tissue engineering: a review, Engineering 7 (7) (2021) 966–978.
[35] A. Li, J. Nicolas, S. Mura, Unlocking the potential of hybrid nanocomposite hydrogels: design, mechanical properties and biomedical performances, ChemRxiv 2024 (1021) (2024).
[36] V. De Matteis, Exposure to inorganic nanoparticles: routes of entry, immune response, biodistribution and in vitro/in vivo toxicity evaluation, Toxics 5 (4) (2017) 29.
[37] O. Marciano, S. Gonen, N. Levy, E. Teblum, R. Yemini, G.D. Nessim, S. Ruthstein, L. Elbaz, Modulation of oxygen content in graphene surfaces using temperature-programmed reductive annealing: electron paramagnetic resonance and electrochemical study, Langmuir 32 (44) (2016) 11672–11680.
[38] L. Vannozzi, E. Catalano, M. Telkhozhayeva, E. Teblum, A. Yarmolenko, E. S. Avraham, R. Konar, G.D. Nessim, L. Ricotti, Graphene oxide and reduced graphene oxide nanoflakes coated with glycol chitosan, propylene glycol alginate, and polydopamine: characterization and cytotoxicity in human chondrocytes, Nanomaterials (2021).
[39] D.F. Coutinho, S.V. Sant, H. Shin, J.T. Oliveira, M.E. Gomes, N.M. Neves, A. Khademhosseini, R.L. Reis, Modified gellan gum hydrogels with tunable physical and mechanical properties, Biomaterials 31 (29) (2010) 7494–7502.
[40] D. Trucco, L. Riacci, L. Vannozzi, C. Manferdini, L. Arrico, E. Gabusi, G. Lisignoli, L. Ricotti, Primers for the adhesion of gellan gum-based hydrogels to the cartilage: a comparative study, Macromol. Biosci. 22 (10) (2022) 2200096.
[41] Daniele Guarnera, Francesco Restaino, Lorenzo Vannozzi, Diego Trucco, Tommaso Mazzocchi, Michał Worwąg, Tomasz Gapinski, Gina Lisignoli, Stefano Zaffagnini, Alessandro Russo, L. Ricotti, Arthroscopic device with bendable tip for the controlled extrusion of hydrogels on cartilage defects, Scientific reports (2024).
[42] J.P. Denier, P.P. Dabrowski, On the boundary–layer equations for power–law fluids, Proceedings of the Royal Society of London. Series A: Mathematical, Physical and Engineering Sciences 460(2051) (2004) 3143-3158.
[43] D. Trucco, A. Sharma, C. Manferdini, E. Gabusi, M. Petretta, G. Desando, L. Ricotti, J. Chakraborty, S. Ghosh, G. Lisignoli, Modeling and fabrication of silk fibroin–gelatin-based constructs using extrusion-based three-dimensional bioprinting, ACS Biomater Sci. Eng. 7 (7) (2021) 3306–3320.
[44] A.J. Smith, R.E. Clutton, E. Lilley, K.E.A. Hansen, T. Brattelid, PREPARE: guidelines for planning animal research and testing, Lab. Anim 52 (2) (2018) 135–141.
[45] N. Percie du Sert, V. Hurst, A. Ahluwalia, S. Alam, M.T. Avey, M. Baker, W.J. Browne, A. Clark, I.C. Cuthill, U. Dirnagl, M. Emerson, P. Garner, S.T. Holgate, D. W. Howells, N.A. Karp, S.E. Lazic, K. Lidster, C.J. MacCallum, M. Macleod, E.J. Pearl, O.H. Petersen, F. Rawle, P. Reynolds, K. Rooney, E.S. Sena, S.D. Silberberg, T. Steckler, H. Würbel, The ARRIVE guidelines 2.0: Updated guidelines for reporting animal research, Journal of cerebral blood flow and metabolism : official journal of the International Society of Cerebral Blood Flow and Metabolism 40(9) (2020) 1769-1777.
[46] B. Magnusson, A.M. Kligman, The identification of contact allergens by animal assay. The guinea pig maximization test, J. Investig. Dermatol. 52 (3) (1969) 268–276.
[47] Y. Henrotin, Y. Henrotin, R. Bannuru, M. Malaise, H.-K. Ea, C. Confavreux, J. Bentin, D. Urbin-Choffray, T. Conrozier, J.-P. Brasseur, P. Thomas, A.-C. Hick, A. Marinello, N. Giordan, P. Richette, Hyaluronan derivative HYMOVIS® increases cartilage volume and type ii collagen turnover in osteoarhritic knee: data from MOKHA study, BMC Musculoskelet. Disord. (2019) 293.
[48] O.M. Russu, T.S. Pop, A.M. Feier, C. Trâmbițaș, Z. Incze-Bartha, P.G. Borodi, I. Gergely, S.G. Zuh, Treatment efficacy with a novel hyaluronic acid-based hydrogel for osteoarthritis of the knee, J. Personal. Med. 11 (4) (2021).
[49] D.-A. Wang, S. Varghese, B. Sharma, I. Strehin, S. Fermanian, J. Gorham, D. H. Fairbrother, B. Cascio, J.H. Elisseeff, Multifunctional chondroitin sulphate for cartilage tissue–biomaterial integration, Nat. Mater. 6 (5) (2007) 385–392.
[50] G. O'Connell, J. Garcia, J. Amir, 3D bioprinting: new directions in articular cartilage tissue engineering, ACS Biomater Sci. Eng. 3 (11) (2017) 2657–2668.
[51] C. Petterino, A. Argentino-Storino, Clinical chemistry and haematology historical data in control Sprague-Dawley rats from pre-clinical toxicity studies, Exp. Toxicol. Pathol. 57 (3) (2006) 213–219.
[52] M. Giknis, C. Clifford, Clinical Laboratory Parameters for Crl:CD(SD) Rats, Charles River Laboratories https://www.criver.com/resources/rmrmrclinicalparametersc drat06 (2006).
[53] A.K. Dubey, G. Thrivikraman, B. Basu, Absence of systemic toxicity in mouse model towards BaTiO3 nanoparticulate based eluate treatment, J. Mater. Sci. – Mater. Med. 26 (2) (2015) 103.
[54] G. Ciofani, L. Ricotti, C. Canale, D. D'Alessandro, S. Berrettini, B. Mazzolai, V. Mattoli, Effects of barium titanate nanoparticles on proliferation and differentiation of rat mesenchymal stem cells, Colloids Surf. B, Biointerfaces 102 (2013) 312–320.
[55] A. Blaeser, D.F. Duarte Campos, U. Puster, W. Richtering, M.M. Stevens, H. Fischer, Controlling shear stress in 3D bioprinting is a key factor to balance printing resolution and stem cell integrity, Adv. Healthc. Mater. 5 (3) (2016) 326–333.

[56] J. Aigoin, B. Payré, J. Minvielle Moncla, M. Escudero, D. Goudouneche, D. Ferri-Angulo, P.-F. Calmon, L. Vaysse, P. Kemoun, L. Malaquin, J. Foncy, Comparative analysis of electron microscopy techniques for hydrogel microarchitecture characterization: SEM, Cryo-SEM, ESEM, and TEM, ACS Omega 10 (15) (2025) 14687–14698.
[57] B. Parshad, X. Hu, I. Nagle, S.S. Rajput, F. Peng, E. Roussakis, J.P. Cascales, T. McPartland, A. Wiatrowski, J.B. Slade, T. Nguyen, R.S. Knipe, M.W. Grinstaff, C. L. Evans, Hydrogel nanocomposite-based breathable non-adhesive coating for oxygen sensing film used within extracorporeal perfusion system, Sci. Rep. 15 (1) (2025) 38734.
[58] R. Wang, C. Cheng, H. Wang, D. Wang, Swollen hydrogel nanotechnology: advanced applications of the rudimentary swelling properties of hydrogels, ChemPhysMater 3 (4) (2024) 357–375.
[59] H. Yao, H. Liu, X. Cui, Z. Zhao, M. Wang, D. Lu, Key Strategies to improve the mechanical strength and toughness of hydrogels: a review, ACS Appl. Mater. Interfaces 18 (12) (2026) 17253–17292.
[60] Y. Zhao, B. Ran, D. Lee, J. Liao, Photo-controllable smart hydrogels for biomedical application: a review, Small Methods 8 (1) (2024) 2301095.
[61] I.C. Amaechi, G. Kolhatkar, A.H. Youssef, D. Rawach, S. Sun, A. Ruediger, B-site modified photoferroic Cr3+-doped barium titanate nanoparticles: microwave-assisted hydrothermal synthesis, photocatalytic and electrochemical properties, RSC Adv. 9 (36) (2019) 20806–20817.
[62] A. Alangari, F.M. Aldakheel, A. Mateen, M.S. Alqhatani, A.L. Alaofi, M. Shahid, R. Ali, R. Syed, S.F. Adil, M. Khan, M. Kuniyil, M.R. Shaik, Assessment of physicochemical, anticancer, antimicrobial, and biofilm activities of N-doped graphene, Crystals 12 (8) (2022) 1035.
[63] M.C. Arno, M. Inam, A.C. Weems, Z. Li, A.L.A. Binch, C.I. Platt, S.M. Richardson, J. A. Hoyland, A.P. Dove, R.K. O'Reilly, Exploiting the role of nanoparticle shape in enhancing hydrogel adhesive and mechanical properties, Nat. Commun. 11 (1) (2020) 1420.
[64] Y. Zhang, C. Wu, S. Guo, J. Zhang, Interactions of graphene and graphene oxide with proteins and peptides, Nanotechnol. Rev. 2 (1) (2013) 27–45.
[65] R.A. Greenwald, A.S. Josephson, H.S. Diamond, A. Tsang, Human cartilage lysozyme, J. Clin. Invest. 51 (9) (1972) 2264–2270.
[66] S. Xiao, T. Zhao, J. Wang, C. Wang, J. Du, L. Ying, J. Lin, C. Zhang, W. Hu, L. Wang, K. Xu, Gelatin methacrylate (GelMA)-based hydrogels for cell transplantation: an effective strategy for tissue engineering, Stem Cell Rev. Rep. 15 (5) (2019) 664–679.
[67] S. Gruber, A. Nickel, Toxic or not toxic? The specifications of the standard ISO 10993-5 are not explicit enough to yield comparable results in the cytotoxicity assessment of an identical medical device, Front. Med. Technol. 5 (2023) 1195529.
[68] Ó. Cebadero-Dominguez, C. Medrano-Padial, M. Puerto, S. Sánchez-Ballester, A. M. Cameán, Á. Jos, Genotoxicity evaluation of graphene derivatives by a battery of in vitro assays, Chem. Biol. Interact. 372 (2023) 110367.
[69] S. Achawi, J. Pourchez, B. Feneon, V. Forest, Graphene-based materials in vitro toxicity and their structure-activity relationships: a systematic literature review, Chem. Res. Toxicol. 34 (9) (2021) 2003–2018.
[70] K. Wu, Q. Zhou, S. Ouyang, Direct and Indirect Genotoxicity of Graphene Family Nanomaterials on DNA-A Review, Nanomaterials (Basel, Switzerland) 11(11) (2021).
[71] S. Bengtson, K. Kling, A.M. Madsen, A.W. Noergaard, N.R. Jacobsen, P.A. Clausen, B. Alonso, A. Pesquera, A. Zurutuza, R. Ramos, H. Okuno, J. Dijon, H. Wallin, U. Vogel, No cytotoxicity or genotoxicity of graphene and graphene oxide in murine lung epithelial FE1 cells in vitro, Environ. Mol. Mutagen. 57 (6) (2016) 469–482.
[72] G. Lippi, T. Meschi, L. Borghi, Mean platelet volume increases with aging in a large population study, Thromb. Res. 129 (4) (2012) e159–e160.
[73] S. Patel, S. Patel, A. Kotadiya, S. Patel, B. Shrimali, N. Joshi, T. Patel, H. Trivedi, J. Patel, A. Joharapurkar, M. Jain, Age-related changes in hematological and biochemical profiles of Wistar rats, Lab. Anim. Res. 40 (1) (2024) 7.
[74] Q. He, G. Su, K. Liu, F. Zhang, Y. Jiang, J. Gao, L. Liu, Z. Jiang, M. Jin, H. Xie, Sex-specific reference intervals of hematologic and biochemical analytes in Sprague-Dawley rats using the nonparametric rank percentile method, PLoS One 12 (12) (2017) e0189837.
[75] A.K. Patlolla, J. Rondalph, P.B. Tchounwou, Biochemical and histopathological evaluation of graphene oxide in sprague-dawley rats, Austin J. Environ. Toxicol. 3 (1) (2017).
[76] S. Vimalraj, Alkaline phosphatase: Structure, expression and its function in bone mineralization, Gene 754 (2020) 144855.
[77] M.D. Levitt, S.M. Hapak, D.G. Levitt, Alkaline phosphatase pathophysiology with emphasis on the seldom-discussed role of defective elimination in unexplained elevations of serum ALP – A case report and literature review, Clin. Exp. Gastroenterol. 15 (2022) 41–49.
[78] L. Ghiasvand Mohammadkhani, M. Khoshkam, M. Kompany-Zareh, M. Amiri, A. Ramazani, Metabolomics approach to study in vivo toxicity of graphene oxide nanosheets, J. Appl. Toxicol. 42 (3) (2022) 506–515.
[79] Y. Piao, Y. Liu, X. Xie, Change trends of organ weight background data in sprague dawley rats at different ages, J. Toxicol. Pathol. 26 (1) (2013) 29–34.
[80] E. Sartip, T. Behzad, M. Kharaziha, Fabrication and characterization of 3D printed agarose/poly(ethylene glycol) diacrylate/hydroxyapatite nanocomposite hydrogel for cartilage tissue engineering, Int. J. Biol. Macromol. 320 (Pt 2) (2025) 145573.
[81] X. Feng, Y. Fang, H. Yu, Y. Wang, Y. Xu, C. Shi, H. Xia, R.K. Kankala, A. Chen, S. Wang, C. Fu, Injectable Chondroitin Sulfate Methacrylate Hydrogel Microspheres Co-Loaded with GLPM Nanozyme, Dexamethasone, and Stem Cells for Synergistic Osteoarthritis Therapy, Advanced science (Weinheim, Baden-Wurttemberg, Germany) (2026) e17083.
[82] P. Wang, H. Zhao, S. Zhang, Y. Guo, X. Xing, S. Zhou, S. Yang, F. Wang, W. Chen, J. Wang, Y. Zhang, Injectable microgels carrying engineered biomimetic nanoparticles for osteoarthritis therapy via dual-targeted senescent chondrocyte clearance and endogenous repair promotion, Bioact. Mater. 58 (2026) 486–504.
[83] K. Zhou, X. He, K. Shi, D. Hu, C. Yang, M. Gao, Y. Wang, Y. Liu, Q. Yang, B. Chu, J. Peng, Z. Qian, A dual responsive nanohydrogel system for sustained drug delivery and cartilage penetration in osteoarthritis therapy, J. Control. Release 389 (2026) 114494.
[84] A.H. Mota, R. Direito, M.P. Carrasco, P. Rijo, L. Ascensão, A.S. Viana, J. Rocha, M. Eduardo-Figueira, M.J. Rodrigues, L. Custódio, N. Kuplennik, A. Sosnik, A. J. Almeida, M.M. Gaspar, C.P. Reis, Combination of hyaluronic acid and PLGA particles as hybrid systems for viscosupplementation in osteoarthritis, Int. J. Pharm. 559 (2019) 13–22.
[85] M. Abtahi, S.N. Khorasani, S. Khalili, M. Hafezi, M. Sattari-Najafabadi, M. Chahi, R. E. Neisiany, IPN nanocomposite scaffolds based on GelMA-alginate with modified super-paramagnetic iron oxide for cartilage tissue engineering, Int. J. Biol. Macromol. 311 (Pt 2) (2025) 143845.
[86] Y. Liu, G. Dzidotor, T.T. Le, T. Vinikoor, K. Morgan, E.J. Curry, R. Das, A. McClinton, E. Eisenberg, L.N. Apuzzo, K.T.M. Tran, P. Prasad, T.J. Flanagan, S. W. Lee, H.M. Kan, M.T. Chorsi, K.W.H. Lo, C.T. Laurencin, T.D. Nguyen, Exercise-induced piezoelectric stimulation for cartilage regeneration in rabbits, Sci. Transl. Med. 14 (627) (2022) eabi7282.
[87] T. Vinikoor, G.K. Dzidotor, T.T. Le, Y. Liu, H.-M. Kan, S. Barui, M.T. Chorsi, E. J. Curry, E. Reinhardt, H. Wang, P. Singh, M.A. Merriman, E. D'Orio, J. Park, S. Xiao, J.H. Chapman, F. Lin, C.-S. Truong, S. Prasadh, L. Chuba, S. Killoh, S.-W. Lee, Q. Wu, R.M. Chidambaram, K.W.H. Lo, C.T. Laurencin, T.D. Nguyen, Injectable and biodegradable piezoelectric hydrogel for osteoarthritis treatment, Nat. Commun. 14 (1) (2023) 6257.
[88] M. Gong, J. Sun, G. Liu, L. Li, S. Wu, Z. Xiang, Graphene oxide–modified 3D acellular cartilage extracellular matrix scaffold for cartilage regeneration, Mater. Sci. Eng. C 119 (2021) 111603.
[89] V. Nazar, M. Kashi, M. Haghbin Nazarpak, E. Shahryari, M. Mehrjoo, Gelatin hydrogel reinforced by graphene oxide grafted chitosan for cartilage tissue engineering application, Int. J. Polym. Mater. Polym. Biomater. 72 (14) (2023) 1120–1131.
[90] M.B. Jalageri, G.C.M. Kumar, Graphene oxide reinforced polyvinyl alcohol/Chitosan composite hydrogel for cartilage regeneration, Polym. Bull. 81 (12) (2024) 10915–10932.
[91] P. Karami, C.S. Wyss, A. Khoushabi, A. Schmocker, M. Broome, C. Moser, P.-E. Bourban, D.P. Pioletti, Composite double-network hydrogels to improve adhesion on biological surfaces, ACS Appl. Mater. Interfaces 10 (45) (2018) 38692–38699.
[92] A.F. Amhare, L. Qiao, H. Deng, J. Lin, J. Wang, W. Wang, J. Han, The current status of nano-hydrogel preparations for osteochondral repair: Systematic Review, Front. Bioeng. Biotechnol. 13 (2025) 1611522.
[93] Y. Ao, E. Zhang, Y. Liu, L. Yang, J. Li, F. Wang, Advanced hydrogels with nanoparticle inclusion for cartilage tissue engineering, Front. Bioeng. Biotechnol. 10 (2022) 951513.
[94] S. Parveen, S.B. Bozal, J.S. Pober, W.M. Saltzman, Nanoparticle-hydrogel composites for precision medicine, Cell Biomater. (2026) 100372.
[95] K.L. Bennell, K.L. Paterson, B.R. Metcalf, V. Duong, J. Eyles, J. Kasza, Y. Wang, F. Cicuttini, R. Buchbinder, A. Forbes, A. Harris, S.P. Yu, D. Connell, J. Linklater, B. H. Wang, W.M. Oo, D.J. Hunter, Effect of intra-articular platelet-rich plasma vs placebo injection on pain and medial tibial cartilage volume in patients with knee osteoarthritis: the RESTORE randomized clinical trial, J. Am. Med. Assoc. 326 (20) (2021) 2021–2030.
[96] M. Simental-Mendía, D. Ortega-Mata, C.A. Acosta-Olivo, Platelet-rich plasma for knee osteoarthritis: what does the evidence say? Drugs Aging 40 (7) (2023) 585–603.